JAERI-M
7408

ANNUAL REPORT ON NEUTRON SCATTERING STUDIES IN JAERI, JULY, 1976-JUNE, 1977

November 1977

Yoshikazu HAMAGUCHI, Masashi IIZUMI and
Yasuo ENDOH (eds.)

日本原子力研究所
Japan Atomic Energy Research Institute

この報告書は、日本原子力研究所がJAERI-Mレポートとして、不定期に刊行している研究報告書です。入手、複製などのお問合わせは、日本原子力研究所技術情報部（茨城県那珂郡東海村）あて、お申しこしください。

JAERI-M reports, issued irregularly, describe the results of research works carried out in JAERI. Inquiries about the availability of reports and their reproduction should be addressed to Division of Technical Information, Japan Atomic Energy Research Institute, Tokai-mura, Naka-gun, Ibaraki-ken, Japan.

JAERI-M 7408

Annual report on neutron scattering studies in JAERI , July, 1976 - June, 1977

Yoshikazu HAMAGUCHI, Masashi IIZUMI and
Yasuo ENDOH* (eds.)

Division of Physics, Tokai Research
Establishment, JAERI

(Received November 2, 1977)

Neutron scattering studies carried out by Division of Physics,JAERI and by several universities utilizing facilities in Tokai are reported for the period of July, 1976 to June, 1977. The report contains 39 short papers submitted by authors on their individual studies.

Key word;
neutron scattering, neutron diffraction, neutron optics, solid state physics,condensed matters, crystal structure, lattice dynamics, structural phase transition, magnetic structure, magnetic moment distribution, spin wave, liquids, JAERI.

---

* Tohoku University

JAERI－M　7408

原研における中性子散乱研究年次報告
（1976年7月～1977年6月）

日本原子力研究所東海研究所物理部

（編）浜口　由和・飯泉　仁・遠藤　康夫*

（1977年11月2日受理）

JRR－2，3を使い，原研物理部，諸大学研究機関によって行われた中性子散乱研究の，1年間の成果をまとめたもので，39篇の小論文を収録してある。

＊東北大学

PREFACE

This report represents the first attempt in the past fifteen years to summarized the neutron scattering research carried out by using the research reactors (JRR-2 and -3) in Tokai Establishment, Japan Atomic Energy Research Institute (JAERI).

The period covered is the year from July 1, 1976 to June 30, 1977. This was the period of revival of the neutron scattering works in this institute, following immediately the restart of both reactors after extensive and long-lasting repair. During the long shut-down most of the existing neutron spectrometers have been overhauled or rebuilt and a new facility was installed.

Now there are four 3-axis spectrometers, one time-of-flight spectrometer and one neutron diffractometer for topography in JRR-2 and two neutron diffractometers and one polarized-neutron diffractometer are available in JRR-3 (See "Neutron Beam Facilities in Japan, 1975"). Quite recently a new 3-axis spectrometer with general purposes including polarization analysis has been constructed in JRR-2.

Each neutron facility belongs to one of the following four institutes:

Neutron scattering Laboratory, Physics Division, JAERI,
The Institute for Solid State Physics, The University of Tokyo,
Department of Physics, Tohoku University and
The Research Institute for Iron, Steel and Other Metals, Tohoku University.

They are utilized mainly by the scientists of these institutes. Most of the articles in the present report are contributions by these scientists. But parts of the machine time of the university facilities are open for use by the scientists from other universities in Japan and some articles are contributed by them. Editors believe that the number of contributions under this category will increase in future.

Although most of the works presented in this report have been done separately by each group from the institutes and universities,

the report has been organized in accordance with the research fields of the neutron scattering. The editors would like to present them as unified activity in Tokai and to encourage cooperated works among the groups which justify this organization.

The issuance of this report is not intended to constitute publication in a usual sense of the word. Final results will be submitted for publication in regular journals.

Y. Hamaguchi, M. Iizumi (JAERI)
and Y. Endoh (Tohoku University)
Editors.

CONTENTS

III. MAGNETIC STRUCTURES AND MOMENT DISTRIBUTIONS

IV. MAGNETIC EXCITATIONS.

V. LIQUIDS.

VI. NEUTRON OPTICS AND TECHNIQUES.

Studies on the structural relations between the U_4O_9 and U_3O_7 phases

by Norio Masaki

(J A E R I)

The U-O system is one of the most complicated of the binary systems. When UO_2 is oxidized, the UO_2 phase (fluorite-type structure, space group Fm3m) changes to a new phase at the composition $UO_{2.25}$, namely U_4O_9. The transformation is characterized by a good number of weak superlattice reflexions in the diffraction diagram. The neutron diffraction result[1] on the single crystal has led to the conclusion that U_4O_9 has the space group $I4_132$ with a lattice parameter of nearly four times that of UO_2. Briefly, the defects based on the additional oxygen atoms are ordered in long-range within the large $4xa_0$ cell of UO_2.

Oxidation of UO_2 at low temperature may result in the formation of a number of tetragonal phases in the range $UO_{2.3}$ to $UO_{2.4}$, approximating U_3O_7 in composition. No structure determination has yet been published of any of the tetragonal phases. That is due to the difficulties in preparing the sample in single phase in this range.

Table 1 summarizes the X-ray data for the sample of the tetragonal phase, which is prepared on oxidation of UO_2 at 215 °C. The data establish the identity of this sample seems to be the single phase in composition U_3O_7.

In order to study the structural relations between the U_4O_9 and U_3O_7 phases, neutron diffraction experiments were carried out, and the observed patterns are shown in Fig. 1. There is no indication of superlattice formation in the pattern (U_3O_7). The intensities of the Bragg reflexions (U_3O_7) required that the arrangement of the atoms in UO_2 be essentially retained in U_3O_7. Although the location of the additional oxygen atoms in U_3O_7 could not be determined by the Bragg reflexions, the broad diffuse-like scattering conforms that the ordered defects in U_4O_9 phase probably cluster into small groups, rather than being distributed as isolated interstitial point defects.

1) Masaki, N. & Doi, K. (1972) Acta Cryst. B28, 785-791.

Table 1. X-ray data for U_3O_7 phase

hkl	Iobs	Qobs	Qcal	hkl	Iobs	Qobs	Qcal
111	100	0.102	0.102	402	10	0.684	0.684
002	15	0.130	0.130	420	9	0.692	0.692
200	31	0.139	0.139	224	12	0.798	0.798
202	48	0.269	0.269	422	21	0.823	0.823
220	22	0.277	0.277	115	7	0.884	0.884
113	25	0.363	0.362	333	8	0.916	0.917
311	46	0.379	0.379	511	17	0.933	0.933
222	18	0.407	0.407	404	7	1.075	1.075
004	4	0.522	0.521	440	3	1.107	1.108
400	7	0.554	0.554	$a=b=5.374$ Å, $c/a=1.031$			
313	23	0.640	0.640	(true unit cell dimension			
331	22	0.656	0.656	should be $A=\sqrt{2}a/2$, $C=c$)			
204			0.660				

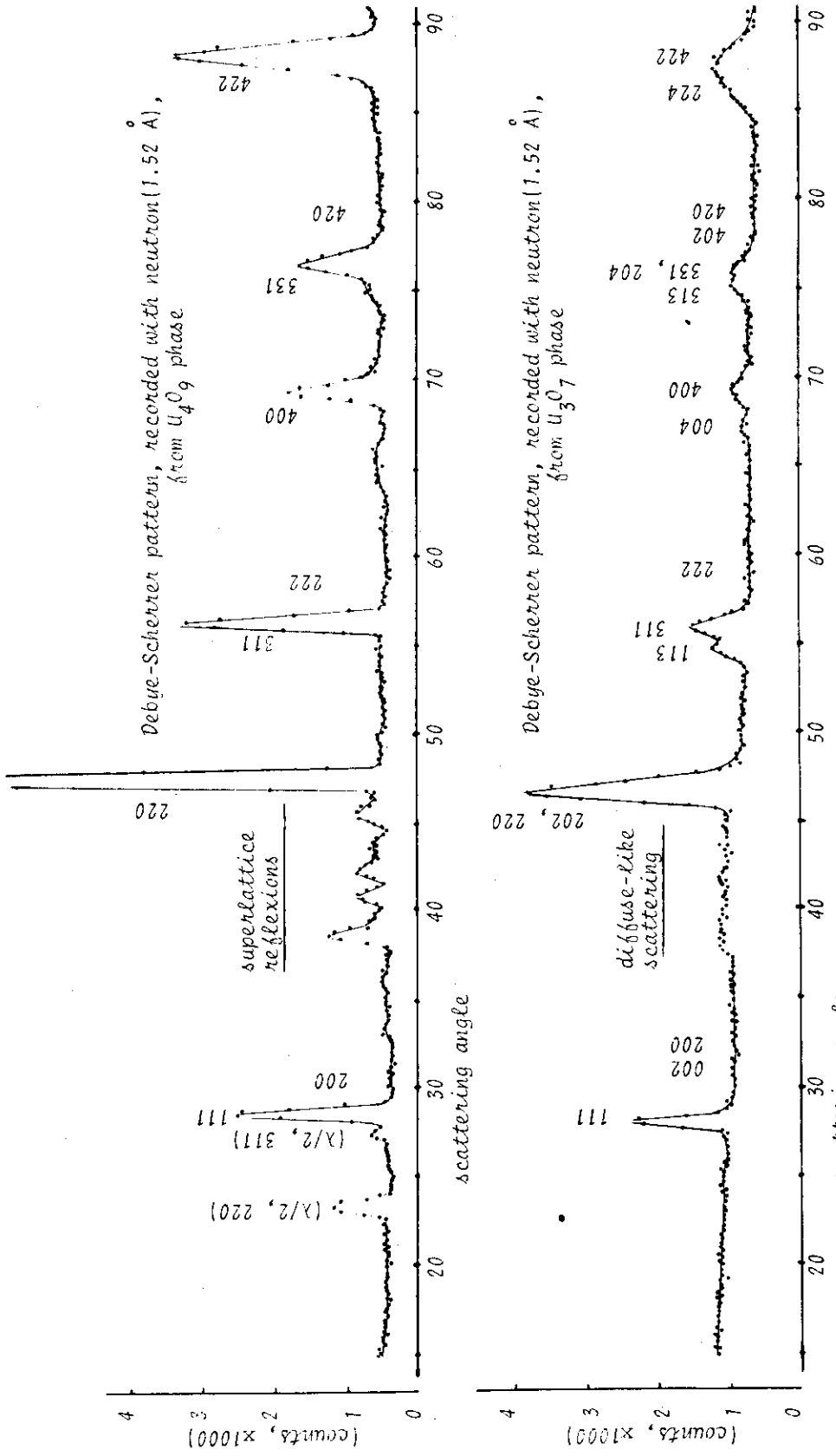

Fig.1. The patterns from the two samples, contained in vanadium holder

DISTRIBUTION AND ANHARMONIC THERMAL VIBRATION OF CATIONS IN α-AgI

S. Hoshino, T. Sakuma and Y. Fujii

Institute for Solid State Physics, The University of Tokyo
Roppongi, Minato-ku, Tokyo 106

Silver iodide in its α-phase above 147°C is known to be a highly conducting solid electrolyte (so-called superionic conductor). The crystal structure is very widely discussed, on account of its having a statistically disordered distribution of cations, and a recent EXAFS study showed that all previous conclusions about the distribution as well as about the dynamics of the cations could be ruled out.

The reexamination of the structure of α-AgI has, therefore, been carried out using data of powder neutron diffraction intensity at 250°C together with X-ray diffraction data. In analysing diffraction data, anharmonic effects in the thermal vibration of the atoms were taken into account. A least squares analysis showed that the experimental data were very well explained by a structure model in which two silver ions are distributed over 12(d) sites of the space group Im3m with large asymmetric anharmonic thermal vibrations. This result is consistent with the EXAFS study by Boyce et al.(1977).

The details have been reported in Solid State Commun. 22 (1977) 763.

A Neutron Diffraction Study of V_2H

by Hajime Asano, Yoshifumi Abe and Makoto Hirabayashi

(The Research Institute for Iron, Steel and Other Metals, Tohoku University)

Hydrogen ordering in metal hydrides has been a favorite subject of neutron diffraction. These studies are made mostly on the deuteride specimens because hydrogen is a strong incoherent scatterer of neutrons. Unfortunately, however, V-H and V-D systems show a remarkable isotope effect in the crystal structure and the phase relation. For example, V_2D exhibits an order-disorder transformation (β-α) of the deuterium arrangement at 130°C, while V_2H undergoes a stepwise phase transition β_1-β_2-α at 175 and 220°C. So we made a neutron diffraction experiment on the powdered hydride specimen to determine the hydrogen locations in β_1- and β_2-V_2H. Measurements were made by using the TOG diffractometer at the JRR-3 reactor.

Figure 1 shows a neutron diffraction pattern of β_1-V_2H at 20°C. In spite of a poor signal-to-noise ratio, two superlattice reflections 001 and 110 + $\bar{1}$10 are clearly seen. The pattern is consistent with the neutron diffraction result on β-V_2D, and the hydrogen arrangement determined is shown in Fig. 2.

The β_1-β_2 transition was studied by the high-temperature examination of the superlattice reflections 001 and 110 + $\bar{1}$10. These reflections disappear at the β_1-β_2 transition point of 175°C, which indicates that the hydrogen atoms in β_2-V_2H distribute among all the o_z-sites (● and x in Fig. 2) with the probability of 1/2.

The structure is a nonstoichiometric form of the superstructure β_2-VH existing over a wide composition range in the phase diagram. This work has been published in J. Phys. Soc. Japan 41 (1976) 974.

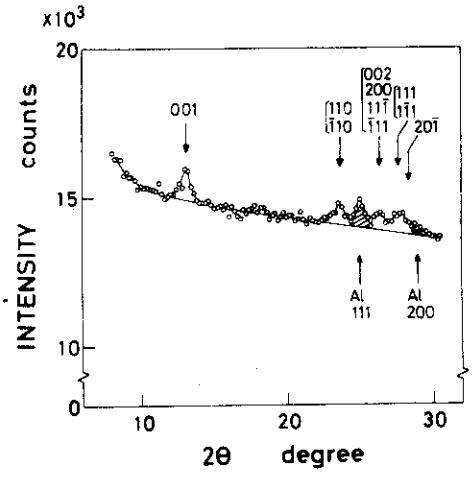

Fig. 1

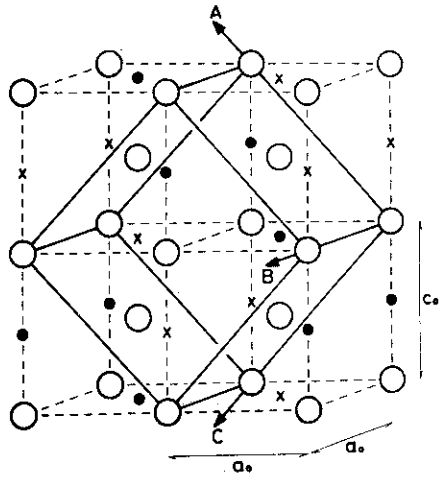

Fig. 2

Fig. [1] Neutron diffraction pattern of β_1-V_2H. λ = 1.02 Å. Shaded reflections come from a sample holder of 0.1 mm -thick aluminum.

Fig. [2] Crystal structure of β_1-V_2H. Open circles represent the vanadium atoms, forming the bct lattice depicted by broken lines. The hydrogen atoms occupy the specific z-type octahedral sites (o_z-sites) shown by full circles. The unit cell of the superlattice is drawn by solid lines.

Locations of Oxygen, Nitrogen and Carbon Atoms in Vanadium Determined by Neutron Diffraction

by Kenji Hiraga, Takashi Onozuka and Makoto Hirabayashi
(The Research Institute for Iron, Steel and Other Metals, Tohoku University)

There has been a great interest for a considerable time in the location of interstitial impurities in b.c.c. metals. Although there is a general belief for the Group-V transition metals that the interstitial atoms enter the octahedral sites, little experimental work has been done to determine directly the interstitial occupancy in these metals.

In the present work, the location of oxygen, nitrogen, and carbon in vanadium have been determined by means of neutron diffraction with the use of single crystals containing of the order of 1 at.% of the interstitial atoms. The neutron diffraction technique is advantageous for the present purpose, because the coherent scattering amplitudes of the interstitial atoms are much larger than that of the vanadium atom; $b_O = 0.575$, $b_N = 0.94$, $b_C = 0.663$ and $b_V = -0.05 \times 10^{-12}$ cm.

Three specimens which are called here $VO_{0.032}$, $VN_{0.013}$, and $VC_{0.006}$, were prepared from appropriate amounts of vanadium metal (99.8%) together with trioxide (V_2O_3), reactor-grade graphite and nonstoichiometric nitride ($\sim VN_{0.8}$), respectively. Each specimen was melted under argon atmosphere in an arc-furnace with a non-consumable electrode. In order to grow large crystals, the ingots were heated at 1600°C for 5 h under vacuum of 10^{-6} Torr, and then

quenched into water from high temperatures. Single crystals of about 1 cm^3 could be grown by this technique. The neutron diffraction study was carried out at room temperature using the TOG diffractometer at JRR-3. The [001] axis of the three crystals was kept normal to the incident beam with the wavelength of about 1.0 Å to measure the intensities of hk0 reflections on the equatorial plane at an angular step of 0.1°.

The neutron diffraction intensities are analyzed by the formula

$$I_{obs} = \frac{KA|F|^2}{\sin 2\theta} \exp\left(-2B \frac{\sin^2\theta}{\lambda^2}\right),$$

where K is a scaling factor, A is the absorption factor which is assumed to be independent of θ, since $\mu R \lesssim 0.2$. For the three crystals, $VO_{0.032}$, $VN_{0.013}$ and $VC_{0.006}$, $\ln(I_{obs} \times \sin 2\theta)^{1/2}$ is plotted as a function of $(\sin\theta/\lambda)^2$ in Fig. 1. The data of every reflection lie on two parallel lines passing through 200-220-400 and 110-310-330. This result indicates that oxygen, nitrogen and carbon atoms in vanadium crystals occupy the octahedral sites randomly, because for the octahedral occupancy there are two kinds of reflections; 200, 220, 222, 400 with the structure factor $b_V + cb_X$, and 110, 211, 310, 321, 330 with $b_V - c/3\, b_X$. The separation of the two parallel lines, which indicates the difference in structure factors for the two kinds of reflections, decreases with decreasing contents of the interstitial atoms in the order of $VO_{0.032}$ - $VN_{0.013}$ - $VC_{0.006}$. Even in the case of $VC_{0.006}$, however, it is still larger than the statistical error of the experimental data which is estimated to be smaller than the radius of open cir-

cles in this figure.

This work has been published in Materials Science and Engineering 27 (1977) 35.

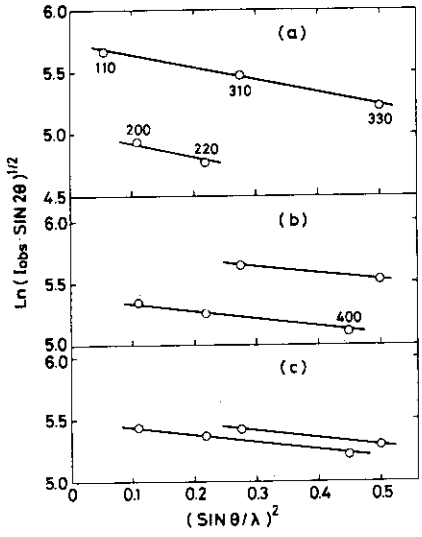

Fig. 1. Observed neutron intensities plotted against $(\sin \theta/\lambda)^2$; (a) $VO_{0.032}$, (b) $VN_{0.013}$ and (c) $VC_{0.006}$.

Neutron Radiation Damage in NbO Single Crystals

by T. Onozuka, M. Koiwa, Y. Ishikawa, S. Yamaguchi
and M. Hirabayashi
(The Research Institute for Iron, Steel and Other Metals,
Tohoku University)

In the study of radiation damage in crystalline solids with energetic particles, the estimation of the number of displaced atoms has been a principal subject of numerous investigations. The purpose of this work is to obtain the quantities of NbO, which has a special crystal structure of a defective NaCl type. This structure is derived from the NaCl cell by taking out an oxygen atom at 0, 0, 0 and a niobium atom at 1/2, 1/2, 1/2, which are called O- and Nb-vacancies, respectively. By virtue of its characteristic structure of NbO, we may evaluate quantitatively irradiation changes in distribution and in concentration of both types of vacant sites from neutron diffraction analyses.

The specimens were irradiated in the Japan Materials Testing Reactor (JMTR) to a total dose of about 1.5×10^{19} nvt of fast neutrons (> 1 MeV). The irradiation temperature was estimated to be lower than 250°C. A disk-shaped crystal of 8 mm diameter, 2 mm thick with the surface parallel to (100) was kept with its [0$\bar{1}$1] direction parallel to the vertical axis of the TOG diffractometer at JRR-3. The wavelength used was about 1.0 Å.

From comparison of the structure factors calculated from several probable models with the observed results, it turns out that a most plausible structure is as follows:

The knock-on atoms fill preferentially their respective vacant sites; oxygen atoms occupy O-vacancies with a probability α, and niobium atoms occupy Nb-vacancies with β.

From the neutron diffraction data, we determined as $\alpha = 0.54$ and $\beta = 0.51$; the O- and Nb-vacancies in the irradiated crystal are occupied with the probability of $\alpha \simeq \beta = 0.5$, and hence the normal atomic positions become statistically vacant with $\alpha/3 = \beta/3 = 0.17$.

It is concluded that the NbO structure tends to change by neutron irradiation towards an imperfect NaCl type containing random vacant sites. The irradiation effects are fully recovered by heating to 900°C.

This work has been published in Radiation Effects 31 (1977) 117.

Neutron Diffraction experiment on γ- $Cu_{15}Mn_{85}$ Single Crystal Alloy

Yoshihiro SHIOZAKI and Yutaka NAKAI
Faculty of Science, Osaka University, Toyonaka
Osaka, 560

1. Introduction Anomalous diffuse scattering has been observed in Cu-Mn alloys over the wide range of Mn concentration (18-90at.%Mn) by neutron diffuraction experiments for powdered samples. These peaks around the (100) scattering angle of f.c.c. structure exist also above the Neel temperature for Mn-rich alloys (>70at.%Mn). Investigations for single crystals[1],[2] without magnetic long range order (MLRO) has ahown that diffuse peaks due to atomic and magnetic short range order (ASRO and MSRO) are found around $(\frac{1}{2}01)$ and its equivalent positions.

We are interested in the mechanism of the formation of MLRO in γ- Cu-Mn alloys and carried out a neutron diffraction experiment on a single crystal with MLRO.

2. Measurements The single crystal was made by Bridgman method; the sample has the following specifications and properties - 10 mm diameter and 30 mm high cylinder, about 85 at.%Mn, $T_N \simeq 410$ K and tetragonality at room temperature $c/a \simeq 0.97$.

Measurements have been performed by TOG diffractometer (double axes and unpolarized neutron scattering) mainly at room temperature except for the study of the temperature dependence of magnetic peaks (110) and diffuse peaks.

Limiting in the 1-st Brillouin zone, we have scanned on (100) and (110) planes, where the length of scattering vectors are larger than 0.6 a*.

In Figure 1 is shown the contour map of scattering intensities on (001) plane with solid curves and zone boundaries with dashed curves. Large diffuse scattering was observed centred about $(\frac{1}{2}01)$; the k-space distribution is

Figure 1

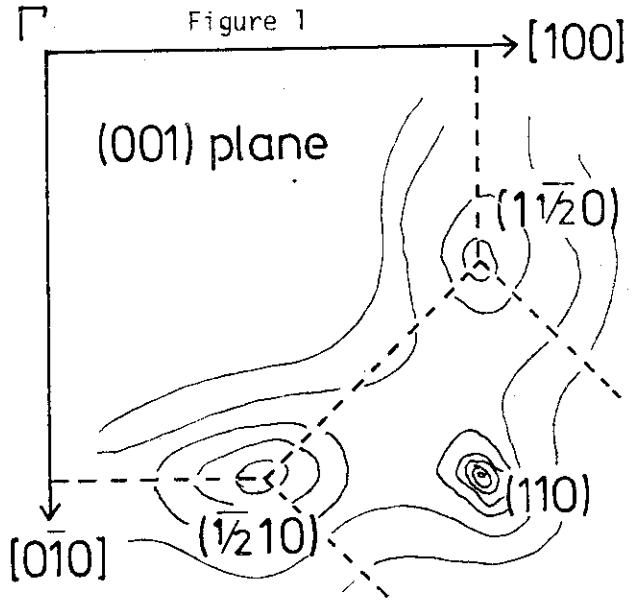

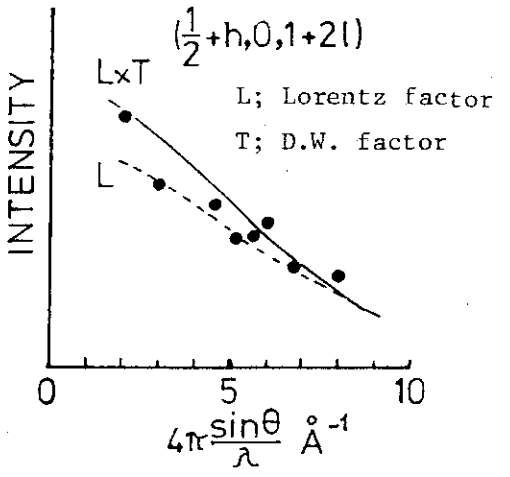

Figure 2

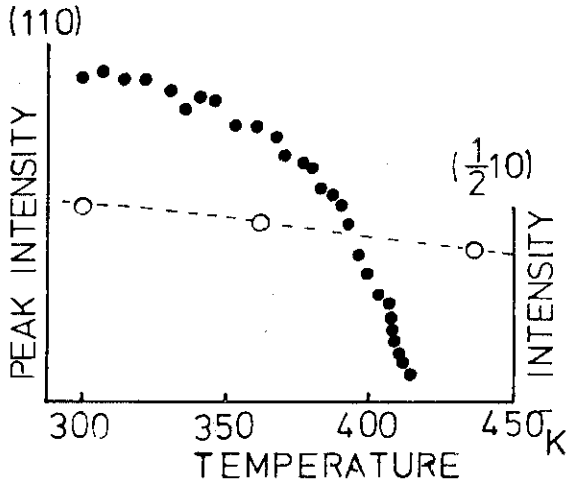

Figure 3

nearly isotropic around $(\frac{1}{2}01)$ with about 0.28 a* FWHM and has cubic symmetry denying the possible contributions from unexpected powder impurities (MnO etc.).

To study the origin of diffuse peaks we have observed h,l-dependence of $(\frac{1}{2}+h,0,1+2l)$ diffuse scattering (Fig.2) and the temperature dependence (Fig.3): From these results, we can conclude that the change of intensities is almost free from the magnetic effects (i.e. magnetic form factor and Neel temperature) and that the atomic short range correlation (DO_{22} type) gives rise to large contributions of diffuse peaks.

3. Results The overall features of diffuse peaks in k-space are similar to those of paramagnetic case, but in that case the magnetic contribution is not small. In spite of the considerble changes in the band structure, Fermi surface and others with varying the alloy composition, the same ASRO structure is observed both in Cu-rich and Mn-rich alloys except the exchange of each position. The origin of ASRO may be direct or very short range interaction.

For an antiferromagnetic γ- Ni-Mn alloy also have been observed large diffuse peaks, but its origin is magnetic and peaks are centred about (100) and its equivalent positions. It is interesting to compare the magnon dispersion curves of these two γ- Mn alloys.

References

(1) P. Wells and J.H. Smith J.Phys. F1 (1971) 763

(2) H. Sato, S.A. Werner and M. Yessik
AIP Conf. Proc. no.5 (1971) 508

Incommensurate Phase Transition in $(ND_4)_2BeF_4$

M. Iizumi and K. Gesi

Physics Division, Japan Atomic Energy Research Institute

The intermediate phase ($T_c < T < T_I$, T_c = 174.5 K, T_I = 179.5 K) of deuterated ammonium fluoberryllate has been found[1] to be incommensurate with the crystal structure in the high temperature phase. The wave vector characterizing satellite reflections deviates slightly from $\vec{q}_X = 0.5\ \vec{a}^*$ characterizing the superlattice structure below T_c and is given by $\vec{q}_\delta = (0.5 - \delta)\ \vec{a}^*$ with the temperature-dependent deviation parameter δ shown in Fig. 1. At T_c δ disappears discontinuously and the crystal transforms to a commensurate structure with spontaneous polarization.

The resemblance of the transitions to those in K_2SeO_4[2] suggests the softening of the Σ_3(TA) - Σ_2 branch around $\vec{q}_X$ above T_I. However neutron scattering measurements in the high temperature phase disclosed a slight change of the

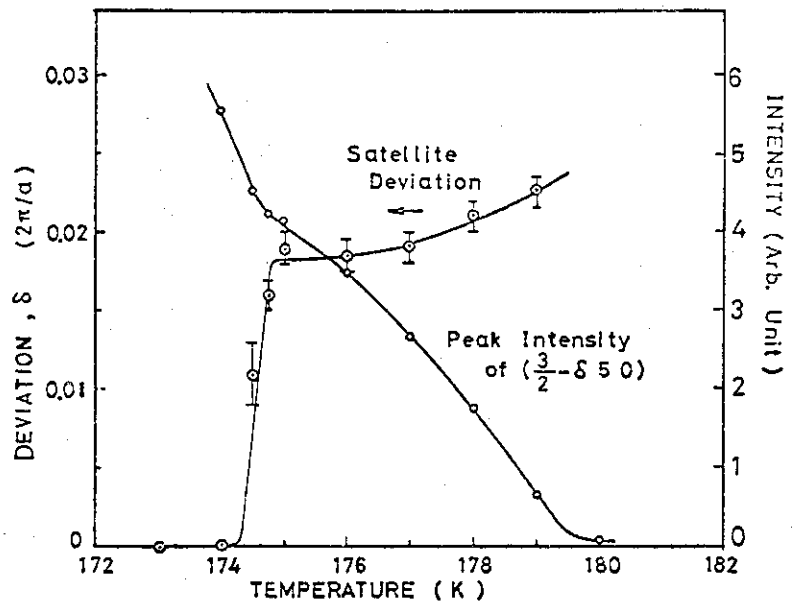

Fig. 1. Temperature change of the parameter δ and peak intensity of $\frac{3}{2} - \delta$ 5 0 satellite reflection.

Incommensurate Phase Transition in $(ND_4)_2BeF_4$

M. Iizumi and K. Gesi

Physics Division, Japan Atomic Energy Research Institute

The intermediate phase ($T_c < T < T_I$, T_c = 174.5 K, T_I = 179.5 K) of deuterated ammonium fluoberryllate has been found[1] to be incommensurate with the crystal structure in the high temperature phase. The wave vector characterizing satellite reflections deviates slightly from $\vec{q}_X = 0.5\ \vec{a}^*$ characterizing the superlattice structure below T_c and is given by $\vec{q}_\delta = (0.5 - \delta)\ \vec{a}^*$ with the temperature-dependent deviation parameter δ shown in Fig. 1. At T_c δ disappears discontinuously and the crystal transforms to a commensurate structure with spontaneous polarization.

The resemblance of the transitions to those in K_2SeO_4[2] suggests the softening of the Σ_3(TA) - Σ_2 branch around $\vec{q}_X$ above T_I. However neutron scattering measurements in the high temperature phase disclosed a slight change of the

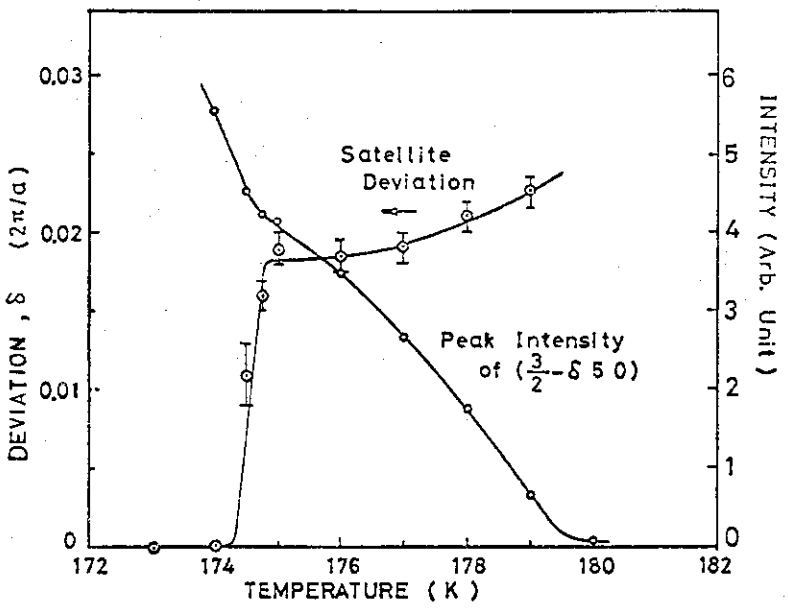

Fig. 1. Temperature change of the parameter δ and peak intensity of $\frac{3}{2} - \delta$ 5 0 satellite reflection.

branch with temperature as is shown in Fig. 2. Instead of the anticipated softening a remarkably temperature-dependent quasi-elastic scattering was observed around $\vec{q}_X$. This has fairly anisotropic distribution around $\vec{q}_X$, extending along [100] with a comparatively narrow width in the perpendicular directions. Peak positions of the scattering along the [100] direction deviate from $\vec{q}_X$ indicating the incommensurate nature of the relevant fluctuations. The energy width of this scattering is very small and resolution-limited. The upper limit of the intrinsic energy-width was estimated to be 0.05 meV by using the 5.0 meV beryllium-filtered incident neutrons.

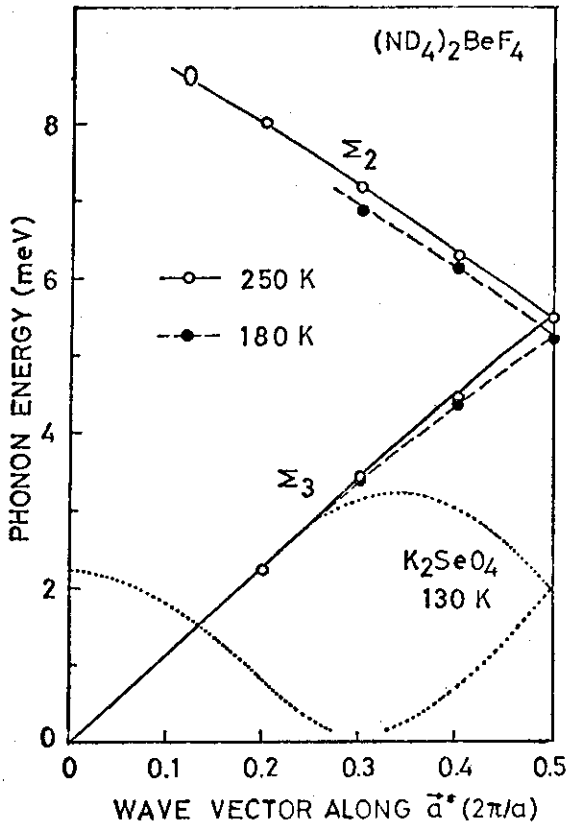

Fig 2. Phonon dispersion relations of low-lying modes of $(ND_4)_2BeF_4$ as compared with those of K_2SeO_4 just above T_I.

Accordingly the dynamical aspects of the incommensurate lattice instability of this substance is fairly different from those in K_2SeO_4. Presumably the fluctuation of the orientation of NH_4 groups coupled with the Σ_2 phonon plays a dominant role in causing the lattice instability. The relaxation of this motion of NH_4 groups is fairly

slow; the relaxation time is estimated to be longer than 1×10^{-10} sec from the energy width of the quasi-eleastic scattering. The mechanisim of locking-in of the commensurate structure and induction of the spontaneous polarization is similar to K_2SeO_4. The significant difference is in the order of the coupling terms which is second in the primary order parameter and linear in the polarization. This explains why the spotaneous polarization is induced in the b direction in this substance.

References

1. M. Iizumi and K. Gesi, Solid State Commun. 22 (1977) 37.
2. M. Iizumi, J. D. Axe, G. Shirane and K. Shimaoka, Phys. Rev. 15 (1977) 4392.

Incommensurate Lattice Instability in Thiourea

Masashi Iizumi and Kazuo Gesi

Physics Division, Japan Atomic Energy Reseach Institute

Thiourea ($SC(NH_2)_2$) is one of the typical substances which exhibit incommensurate structural transitions under current interest. It has three incommensurate phases(II,III and IV) between the ferroelectric phase (I, $T < 169$ K) and the paraelectric phase (V, $T > 202$ K). The incommensurate structures are characterized by satellite reflections of the form $(h,k,\ell\pm n\delta)$ with $n = 1,2,\cdots$. The parameter δ has been measured by Shiozaki[1] for $SC(NH_2)_2$ and by McKenzie[2] for $SC(ND_2)_2$. We have carried out more detailed measurement of δ for the purpose of disclosing any anomaly related to the existence of the phase III, which exhibits spontaneous polarization and is possibly a commensurate phase. The results shown in the Figure 1 do not indicate any evidence of anomalous changes in passing through the phase III. The intensities of satellite do not show any anomaly either. Therefore the three intermediate phases are basically a single incommensurate phase and the spontaneous polarization is induced independently of the incommensurate order patameters in phase III by some other unrevealed mechanism. There is considerable discrepancy in the δ vs. T relation of $SC(NH_2)_2$ between ours and the one obtained by Shiozaki[1] as shown in the fugure. Our result has been confirmed by the recent X-rays measurements[3]. According to our observation there is no isotope effects on the range of δ; both $SC(NH_2)_2$ and $SC(ND_2)_2$ transform to the incommensurate phase with $\delta \approx 1/7$ and the incommensurate-to-commensurate transition takes place at $\delta \approx 1/9$.

Inelastic neutron scattering measurements have been carried out at several temperatures in the phase V of the deuterated samples in order to study the nature of the incommensurate lattice instability. We have been unable to observe any soft branches. The critical scattering with quasielastic nature has been observed around the points where satellites appear below T_{IV-V}(=216.5 K in our samples).

The distribution of the scattering is fairly anisotropic in the Q space with widths being largest in the a* direction and smallest in the b* direction (polar axis in the phase I). The energy profiles of the scattering at $\vec{Q}$ = (0,2,5.2) are shown in the Figure 2 for several temperatures between T_{IV-V} and room temperature. The incoherent scattering shown at the bottom of the figure has been already subtracted. The scattering shows a single peak spectrum between the transition temperature and about 225 K. The width of the scattering changes from 1 meV at 218 K to 1.5 meV at 225 K which are evidently broader than the instrumental resolution of 0.43 meV. Above 230 K the spectrum changes gradually to the double peak structure. The scattering at 300 K is eventually explained by the Λ_4(TA) phonon which is observed with strong intensities around other reciprocal points as shown in the figure. By comparing this profile with those observed at (0,2,5.2) at high temperature, we noticed that the latters are broader in line shape with temperature-dependent intensities. Therefore it is probable to interprete the scattering to consist of the damped soft phonon superposed on the weak TA contributions with interference inbetween.

Further measurements in the phase V and the survey of the phase phonons in the intermediate phases are now in progress.

1) Y. Shiozaki, Ferroelectrics 2 (1971) 245.
2) D. R. McKenzie, J. Phys. C 8 (1975) 1607.
3) H. Takenaka, private communications.

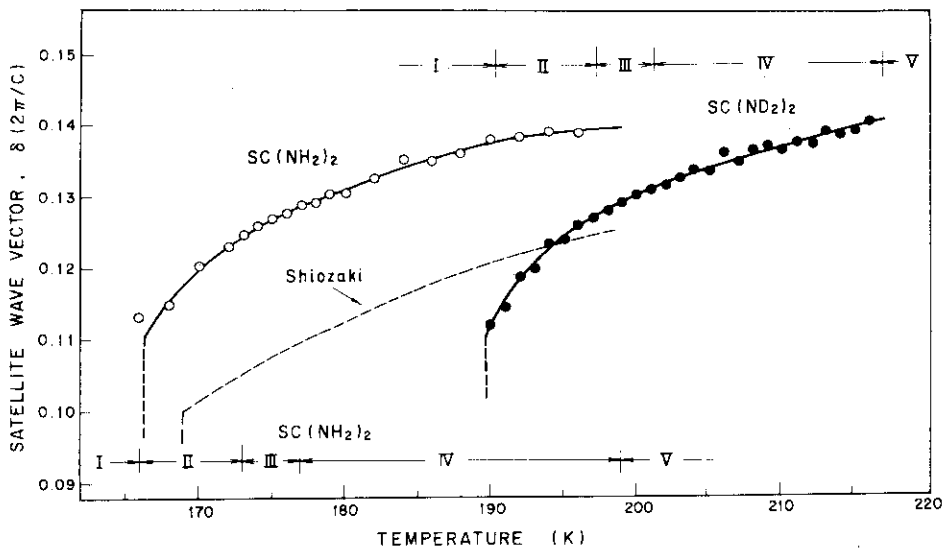

Fig.1 Temperature variation of modulation wave vector

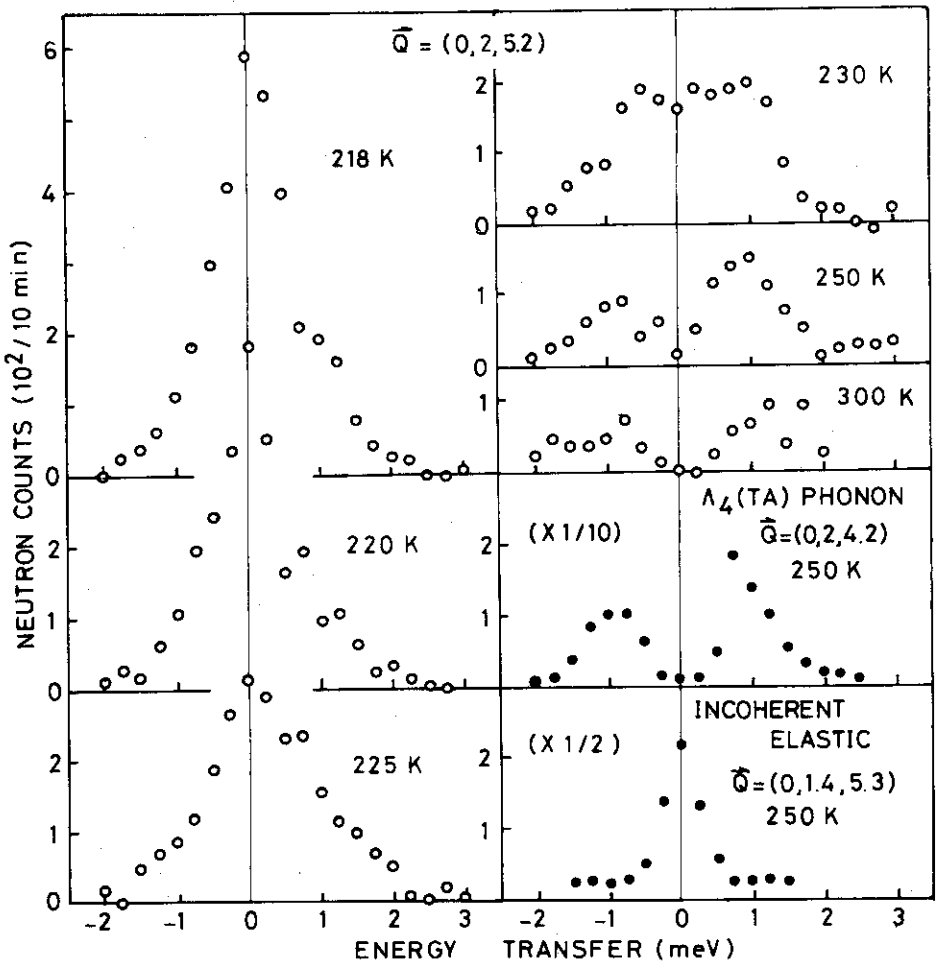

Fig.2 Energy spectra of critical scattering at q = 0.2c*

NEUTRON SCATTERING STUDY OF THE [110] PHONONS IN TlCl

Y. Fujii, T. Sakuma, J. Nakahara, S. Hoshino and K. Kobayashi
Institute for Solid State Physics, The University of Tokyo
Roppongi, Minato-ku, Tokyo 106

and

A. Fujii
Department of Physics, Kumamoto University
Kurokami, Kumamoto 860

Phonon dispersion relations of TlCl having the CsCl type structure have been measured along the [110] direction at 80K, partly at 293K (Fig.1). Four zone-boundary phonons at the M($\frac{1}{2},\frac{1}{2},0$) point associated with the indirect band-gap transition between the X($0,0,\frac{1}{2}$) and R($\frac{1}{2},\frac{1}{2},\frac{1}{2}$) points have been investigated in detail. The optical absorption spectra observed at 2K can be well explained by assigning them to momentum-conserving phonons in this optical transition.

During the course of the present measurement, we found softening of the TA_2 phonon branch ($\vec{e} \parallel [001]$) at the zone-boundary as displayed in Fig.2. TlCl and TlBr show no phase transition while TlI undergoes the cubic-to-orthorhombic transition at 156°C. A stacking of the $(010)_{ortho}$ planes with a sequence of $A^{-}B^{+}ABA^{-}B^{+}AB$ in the low-temperature orthorhombic structure is accomplished by displacing the $(110)_{cubic}$ stacking of ABABABAB in the cubic (CsCl) structure with two waves of wavelengths $2d_{110}$ and $4d_{110}$ where d_{110} is the $(110)_{cubic}$ interplanar spacing. The amplitudes of these two are related by $\sqrt{2}$ and both waves propagate in the [110] direction with polarization in the [001] direction. Then these two waves correspond to the $[110]TA_2$ mode; one has the wave vector $\vec{q}_1 = \frac{1}{2}(1,1,0)$ corresponding to the zone-boundary, the other $\vec{q}_2 = \frac{1}{4}(1,1,0)$. Softening of the $[110]TA_2$ branch observed in TlCl probably shows a premonitory effect of the CsCl-orthorhombic transition realized only in TlI.

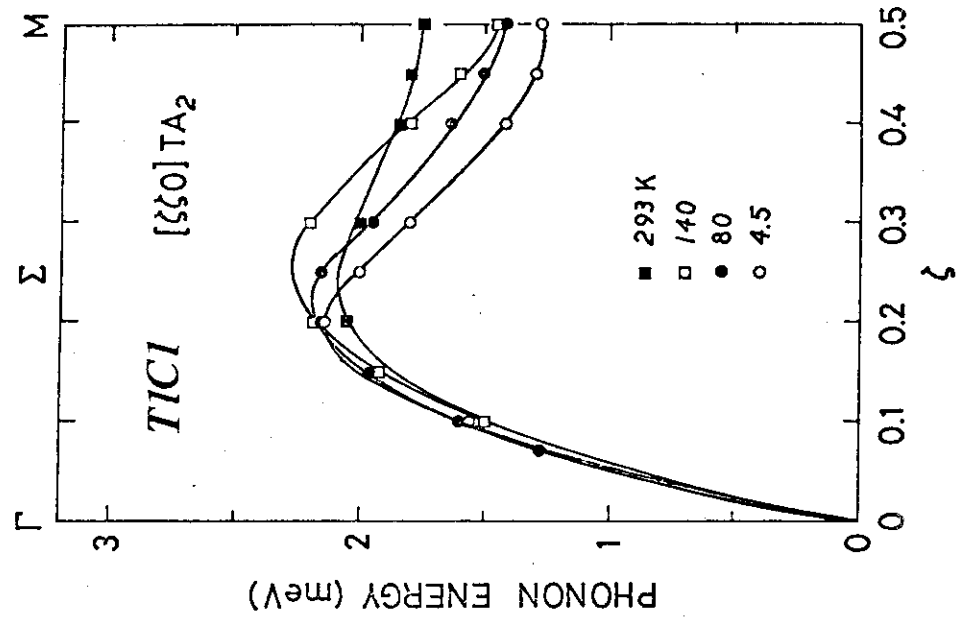
TlCl
[ζ0] TA2
293 K
140
80
4.5
PHONON ENERGY (meV)
ζ
Γ
Σ
M

Fig. 2

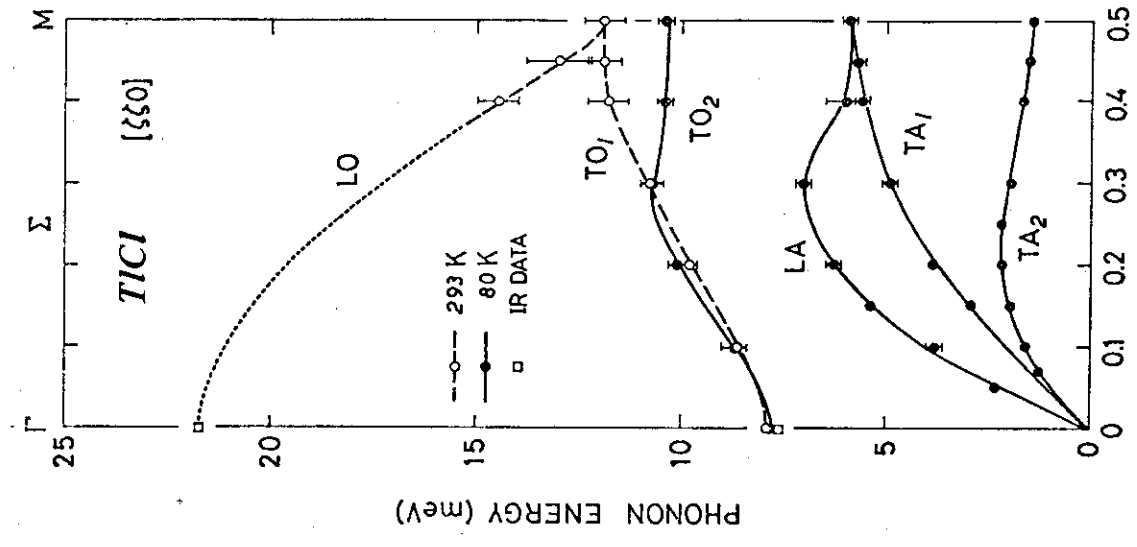
TlCl
[ζ0]
LO
TO1
TO2
LA
TA1
TA2
293 K
80 K
IR DATA
PHONON ENERGY (meV)
ζ
Γ
Σ
M

Fig. 1

Anomalous phonon dispersion in $Fe_{65}Ni_{35}$

by Yasuo Endoh, and Yoshikazu Ishikawa

(Department of Physics, Tohoku University)

The phonon dispersion relations of $Fe_{65}Ni_{35}$ were measured at the room temperature (293 K). The experimental points were analysed in terms of Born-von Kármán model averaging out atomic mass and force constants. Solid lines in the figure represent the results which require 4 neighbours interatomic force constants. The phonon dispersion curve for $[110]T_1$ mode has a noticeable dip. Compared with the earlier results of FeNi alloys by Hallman and Brockhouse, the general agreement is reasonably good except the $[110]T_1$ mode. Since no significant change was found in a force system in range and magnitude among FeNi alloys, the anomalous phonon dispersion of $[110]T_1$ mode in $Fe_{65}Ni_{35}$ is just attributed to the Invar character.

The temperature dependent feature of the anomaly was studied. It turns out that the anomaly is removed above T_C and is pronounced at low temperatures. This gives the direct consequence that the anomaly is associated with the ferromagnetism in the Invar alloy. The elastic softening is also attributed to the lattice dynamical aspects observed in $[110]T_1$ mode.

The temperature dependent dispersion curve of this mode was analyzed in terms of interplaner force constants. This analysis indicated that distant forces are more modified below T_C. Therefore the softening is not dominated by the magnetic exchange coupling between near neighbour atoms, but is influenced by the spin dependent electronic forces.

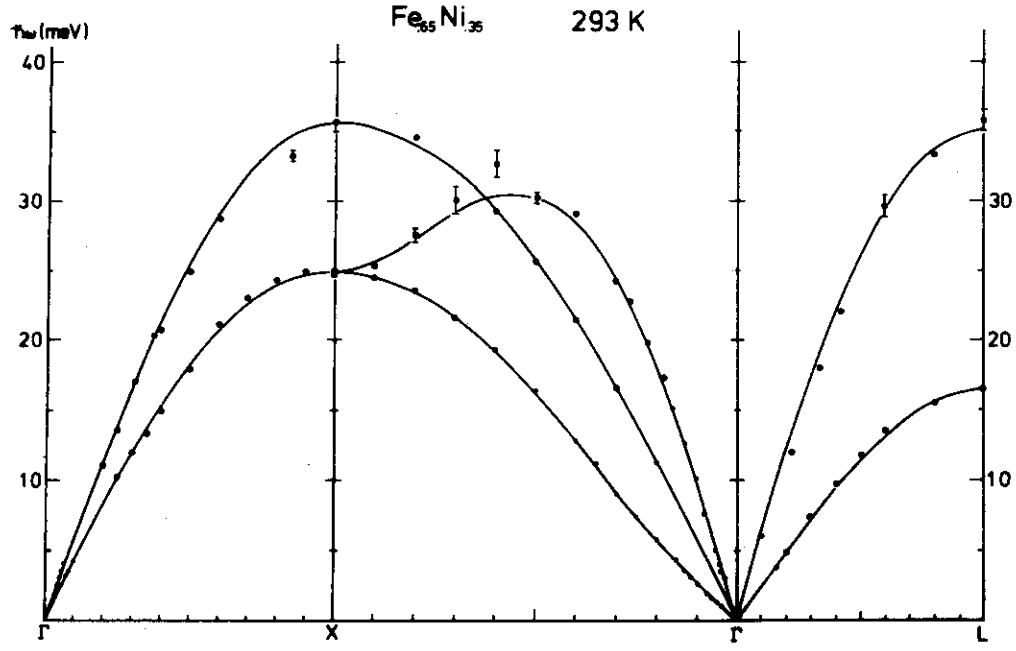

Phonon dispersion curves of $Fe_{65}Ni_{35}$ at room temperature. Experimental errors are in scale of points. Solid lines represent fitting curve in terms of BVK model. (4 neighbour interatomic forces)

Zero Sound Elastic Anomaly in $Fe_{65}Ni_{35}$

by Yasuo Endoh, Kazuyoshi Yamada, and Yoshikazu Ishikawa
(Department of Physics, Tohoku University)
and
Yasuhisa Noda (Sendai Radiotechnical College)

The elastic softening in Invar alloys was focussed which has been revealed by the ultrasonic measurements. A large single crystal of $Fe_{.650}Ni_{.350}$ was used in the experiments. The face centered cubic structure was found to be stable even at 4.2 K. The magnetization studies revealed T_C = 499 ± 2 K. At room temperature the lattice parameter a was determined to be 3.588 ± .002 Å and a changed by a small fraction over a wide range of temperatures studied, which is consistent with the dilatation results. Experiments were performed on TUNS spectrometer at JRR2 with 13.8 meV incident energy. The higher order contaminations were filtered with oriented graphite crystals. All horizontal collimations were 30 minutes. In order to derive the zero sound elastic constants, the phonon dispersions with small phonon wave vectors were taken with careful operation of the spectrometer. As the observed spectrum in a scan is due to a weighted response of all modes within the instrumental resolution, each scan has been analyzed in a way similar to the treatment made in a series of solid rare gas experiments by the Brookhaven group.

The elastic constants were derived by a fitting procedure including the second derivative of the phonon dispersion, $E = \alpha q + \beta q^3$, where α relates to the elastic constants. The results obtained

from [110] phonon modes are illustrated in the figure. The elastic softening is appreciable in the $[110]T_1$ mode below T_C, which is a good agreement with the ultrasonic results. However temperature dependence of the elastic constant for the longitudinal mode disagrees with the ultrasonic results. It is noteworthy that zero sound results are well fitted to the first sound values for $Fe_{49}Ni_{51}$ which has no Invar character.

To conclude, the present studies show that substantial softening of $[110]T_1$ shear modes below T_C is common to the so-called Invar alloys of both FeNi and FePt. Besides, the temperature dependence of the bulk modulus determined from the inelastic neutron scattering is quite similar to that of normal metals. On the contrary, the isothermal bulk modulus of Invar gives a large depression at low temperatures.

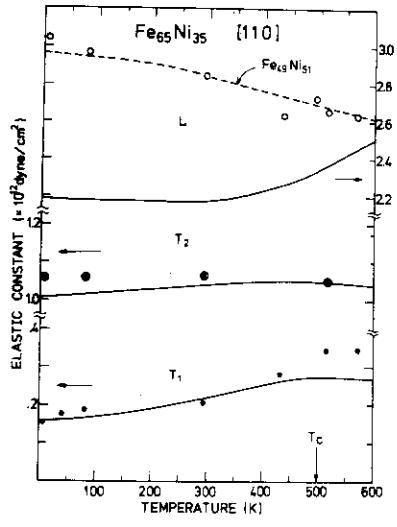

Temperature dependence of elastic constants of various modes along [110]. Points represent zero sound values and lines are first sound ones.

A neutron Scattering Study of the Anharmonicity of Lattice Vibrations and its Relation to the Melting of NaF

H. Yoshizawa and K. Hirakawa

The Institute for Solid State Physics, the University of Tokyo, Roppongi, Minatoku, Tokyo

In connection with the aid of understanding the microscopy of melting phenomena, the lattice vibration of the [110]TA_1 mode in NaF has been studied in detail by neutron inelastic scattering. Our original motivation is simply based on an idea that this mode is most responsible for the melting because the shear modulus $(C_{11} - C_{12})/2$, which could be drawn out from the [110]TA_1 mode, will vanish in the liquid phase, thus one of good extensive variables for the solid liquid transition. Measurements were made starting from the room temperature up to 1250 K which is 98.7% of the melting temperature (T_m = 1266 K). Two quantities, the frequency (ω) shift and the damping constant (2Γ) were studied as functions of various reduced wave number ζ and ω . When the temperature is elevated, an interesting 0 → 1st sound transition could be seen as firstly found by Loidl et al and associated characteristic features of ζ dependence of ω and 2Γ could be observed. In Fig.1, the frequency change for various ζ values is shown. This result shows that frequency shift occurs but near T_m,

neither ω tends to zero nor the temperature derivative to $-\infty$ as $T \rightarrow T_m$. At T_m, ω comes down to about 60% of the low temperature value. This is consistent with the theory of Fukuyama and Platzman based on the self consistent harmonic approximation. The damping constant is shown in Fig.2, in which according to whether the observed phonons are in the 0 sound or in the 1st sound region, characteristic ω(or ζ) dependence of 2Γ is observed. The first sound region is distinguished by the dotted region in which, according to Kwok et al 2Γ is proportional to $\omega^{\sim 2}$, while in the 0 sound region, 2Γ is proportional to ω. These features are clearly seen. Thus the measure of anharmonicity $2\Gamma/\omega$ remains constant at lower temperatures, but with increasing temperatures the 1st sound region extends more and more in wider ζ space and at immediately below T_m, marked anharmonicity is seen at higher ζ mode. This feature is entirely different from the conventional 2nd order transition in which marked fluctuations and anharmonicity can be seen at around $\zeta = 0$ singular point. It is to be pointed out that even at very close to T_m, low ζ modes are surprizingly stable, while higher ζ modes are strongly damped. Physically, this suggests us that near T_m individual atomic (or a small atomic cluster) motions are violent enough but long wave normal modes as in a continuous medium is still maintained. We have got an impression that melting phenomena is not of an instability of collective motions but strongly related to the individual motions of atoms. We may add that no such remarkable features could be seen in the measurements on the [110]TA_2 and [100] TA modes.

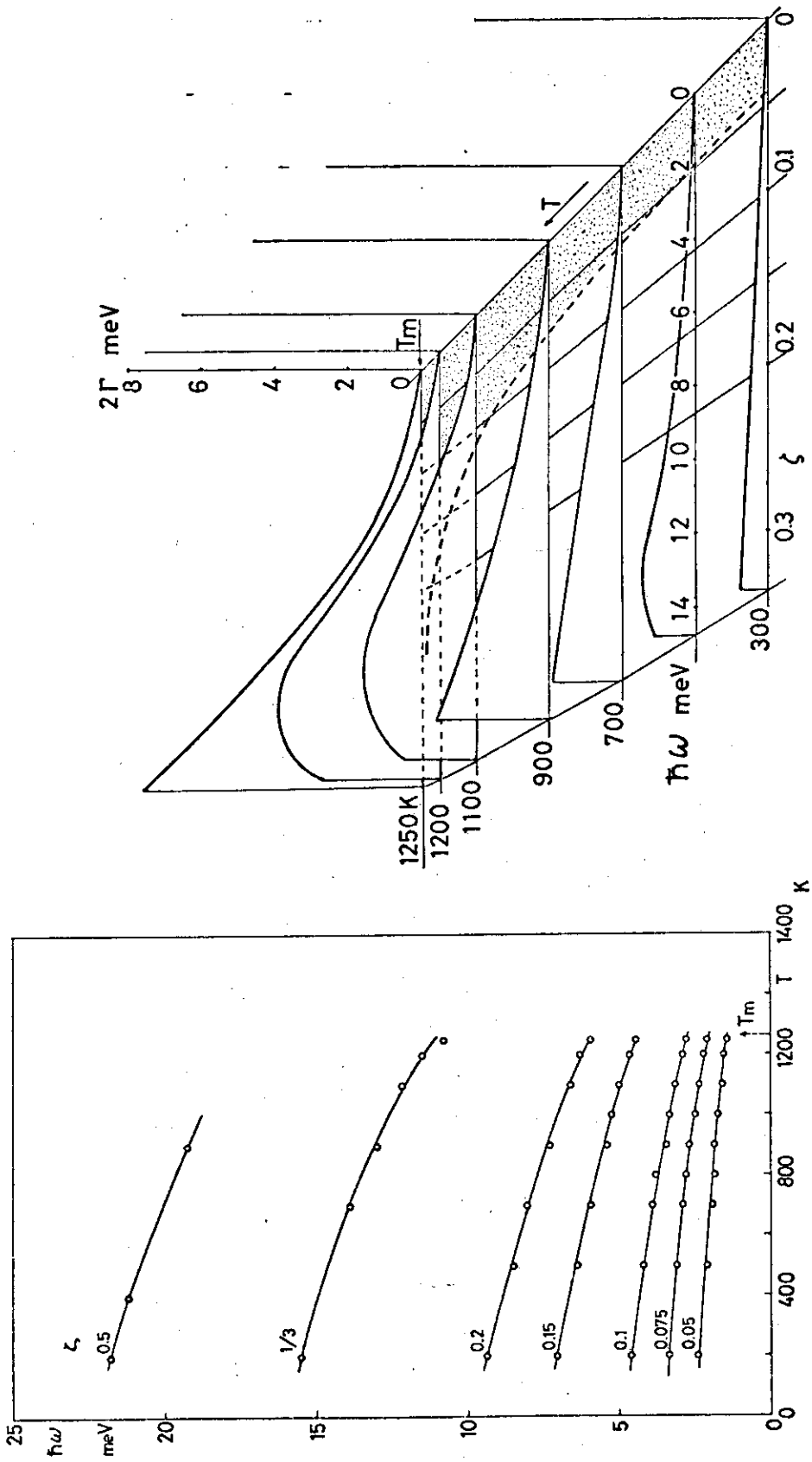
ħω meV
ζ
0.5
1/3
0.2
0.15
0.1
0.075
0.05
Tm
T
K

Fig. 1

2Γ meV
Tm
T
1250K
1200
1100
900
700
ħω meV
300
ζ

Fig. 2

Effect of Precipitation on the Phonons in $Al_{99}Cu$

Nobuhiko KUNITOMI, Mamoru HAMADA and Yutaka NAKAI
Department of Physics, Faculty of Science
Osaka University, Toyonaka, OSAKA, 560

An Al alloy with dilute concentration of Cu is a typical substance which exhibits precipitation phenomena. The early stage of its precipitation has long been a subject of physical and metallurgical researches. It has been known by X-ray diffraction, that a plate of monoatomic layer of Cu called the Preston-Guinier zone is formed by a low temperature anneal and that the interatomic distance in host Al lattice strongly contracts over several atomic layers from the zone. The formation of this deformation field prevents the free motion of dislocations and consequently hardens the material.

In this work, we observed the phonon dispersion relation for $Al_{99}Cu$, expecting to find some modification will take place in the early stage of precipitation due to two reasons, namely (1) change arising from the long range fluctuations of the lattice constant and (2) the appearance or disappearance of the resonance mode.

A single crystal of $Al_{99}Cu$ with cylindrical shape of 16mmϕx250mm was grown by the Bridgeman method from raw materials with the purities of 99.99%. In order to solve Cu into Al completely it was quenched into water from 500°C, and the phonon dispersion relation was observed by neutron inelastic scattering with the use of TUNS. The dispersion relation was again observed after the sample was annealed for 50 hours at 130°C where Preston Guinier zone was grown by this heat-treatment.

In Fig.1 are shown the dispersion relations of this sample with the different heat treatment. It is apparent that the phonon frequency decreases by the precipitation anneal in the region where the wave number of the phonon is relatively large. This implies that there appears some effect of the modification of force constant extending over several atomic distance. Since the experiment was rather preliminary, the existence of the resonance mode was not confirmed.

We are now preparing for further investigations and the analysis of the present results encouraged by the observation of this kind of anomaly.

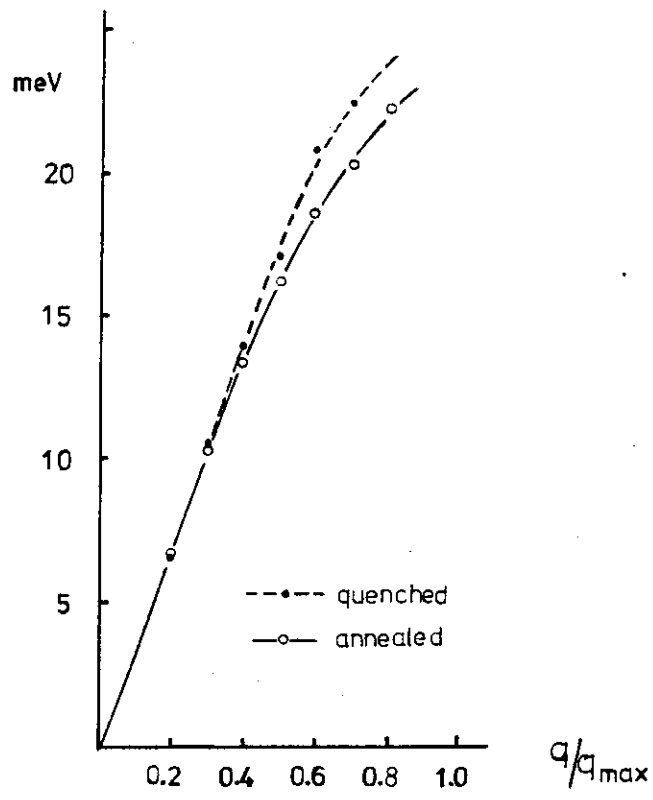

Fig.1. Dispersion Relations

INCOMMENSURATE JAHN-TELLER TRANSITION IN $K_2PbCu(NO_2)_6$

by Yukio Noda, Masahiro Mori and Yasusada Yamada

(College of General Education, Osaka University)

The crystal of $K_2PbCu(NO_2)_6$ undergoes two structural phase transitions successively at 281 and 273 K. The highest temperature phase (Phase I) has cubic symmetry (space group Fm3). These transitions are considered to be the cooperative Jahn-Teller transitions due to the coupling between local 3d electrons of Cu^{2+} and the lattice distortion with local Eg-symmetry [1-3].

Recently, we have performed neutron scattering measurements on this substance at the JAERI CP5 reactor. In the lowest temperature phase (Phase III), we observed super structure reflections at [H±1/2, K±1/2, L±1/2], namely at L-zone boundaries of the Brillouin zone referred to the face centered cubic unit cell. Utilizing lattice dynamical analysis at the L-point, we concluded that the zone boundary phonon which is compatible with the local Jahn-Teller active mode is condensed in Phase III. The resultant structure is an "antiferro-distortive" structure in which the local axis of elongation of $Cu(NO_2)_6$ complex alternates between the a-axis and the b-axis. In terms of pseudospin descriptions of local electronic states, we characterized Phase III as a "canted pseudospin" ordered state.

In the intermediate phase (Phase II), in addition to the tetragonal bulk contraction which was already reported, we observed satellite reflections appearing around each

reciprocal lattice points with indices (H±0.416, K±0.430, 0). Based on this fact, Phase II should be considered as an incommensurate phase with the wave vector $\mathbb{k}_0$=(0.416, 0.430, 0). The direction of $\mathbb{k}_0$ is very close to [110] directions, or the Σ-line of the f.c.c. unit cell. The position of $\mathbb{k}_0$ is close to the middle point between the two commensurate wave vectors; (1/2 1/2 0) and (1/3 1/3 0). The value of $|\mathbb{k}_0|$ does not show appreciable temperature variation throughout Phase II, namely in the temperature range 273K<T<281K. Below 273 K, these satellite reflections completely disappear and instead, the super lattice reflections at (H±1/2, K±1/2, L±1/2) become observalbe.

The structure of Phase II based on the analysis of the satellite intensities is that the local Jahn-Teller distortion is propagating along [110] with $|\mathbb{k}| \simeq 0.42$. The proposed pattern of atomic displacements is depicted in Fig. 1. The most possible candidate of the soft phonon mode propagating along [110] direction is considered to be TA_1-mode (polarized along $[1\bar{1}0]$ since this is compatible with the local Jahn-Teller active mode. Attempts to observe the softening of TA_1 branch in Phase I ($T \gtrsim 281$ K) were made by neutron scattering. However, no well defined TA_1 branch were observed throughout the range of $0.15 < |\mathbb{k}| \lesssim 0.50$. Rather, as is usually the case, strong quasi-elastic streaks were observed running along [110] directions. As the temperature was decreased toward 281 K, the intensity of the quasielastic scattering around $\mathbb{k} \simeq$(1/3 1/3 0) showed an appreciable increase. Upon transition to Phase II, the diffuse intensity suddenly disappeared being replaced by sharp satellite reflections.

It is worthwhile to point out that in terms of pseudospin description of the electronic state, the "spin" structure of Phase II is characterized as a "fan" structure which is seen in the real spin system when the screw spin system is brought into uniform magnetic field perpendicular to the screw axis. This gives an interesting contrast to the spin structure of Phase III which has a "canted spin" order (see Fig. 2).

From structural view point, on the other hand, Phase II is the sinusoidally modulated phase, while Phase III is the antiferro-distortive phase. Therefore the sequencial phase transitions in this crystal is considered as normal→ incommensurate→commensurate structural phase transitions.

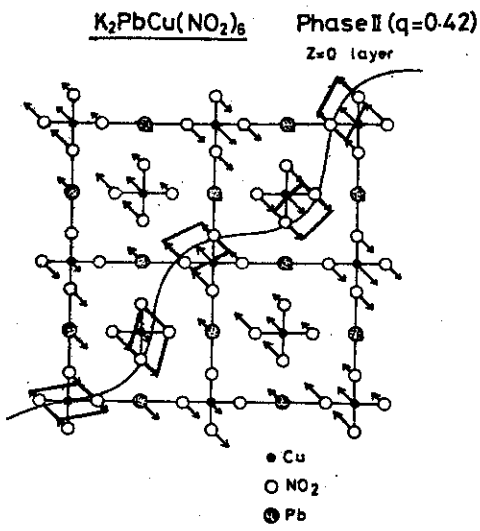

Fig.1. The displacement pattern of TA_1 mode propagating along [110] with the wave vector $|k|=0.42$. Each $Cu(NO_2)_6$ complex shows the distortion which is compatible with local Jahn-Teller active mode

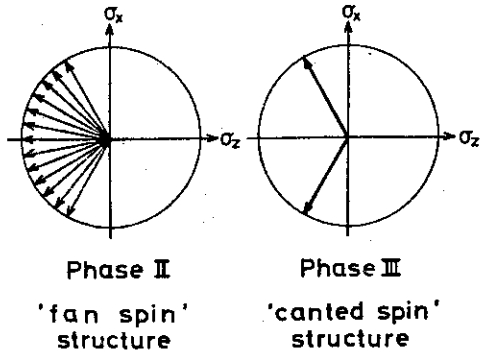

Fig.2. The pseudospin structures in phase II and phase III corresponding to the proposed model structure. The pseudospin structure of phase II is describable as a "fan spin" structure, while phase III as a "canted spin" structure.

QUASIELASTIC NEUTRON SCATTERING FROM SOLID HCl

Y. Fujii, S. Hoshino and T. Sakuma
Institute for Solid State Physics, The University of Tokyo
Roppongi, Minato-ku, Tokyo 106

In the paraelectric phase of solid HCl (T_c=98K <T <T_{mp}=159K), it has a fcc structure with a twelve-fold disordered orientation of molecules directed along the <110> axes. Quasielastic scattering from protons jumping among these twelve <110> directions has been measured as functions of temperature and wave vector Q using a powder sample and the triple-axis neutron scattering technique. The open circles in Fig.1 show the Q-dependence of the quasielastic scattering observed at T=109K. The experimental energy resolution was 0.63 FWHM meV.

The data were well explained by a reorientational jump model in which a proton bound to a chlorine atom (bond length 1.27Å) jumps instantaneously to other positions by 60° or 90° flipping after librating at one position for the residence time τ. The scattering law obtained in this model has only two parameters of τ and the Debye-Waller factor to be varied. The solid curves in Fig.1 are best-fitted ones to the data while the dotted curves show the boundary between the elastic and quasielastic components theoretically obtained. In Fig.2, the residence time so obtained is plotted as a function of temperature.

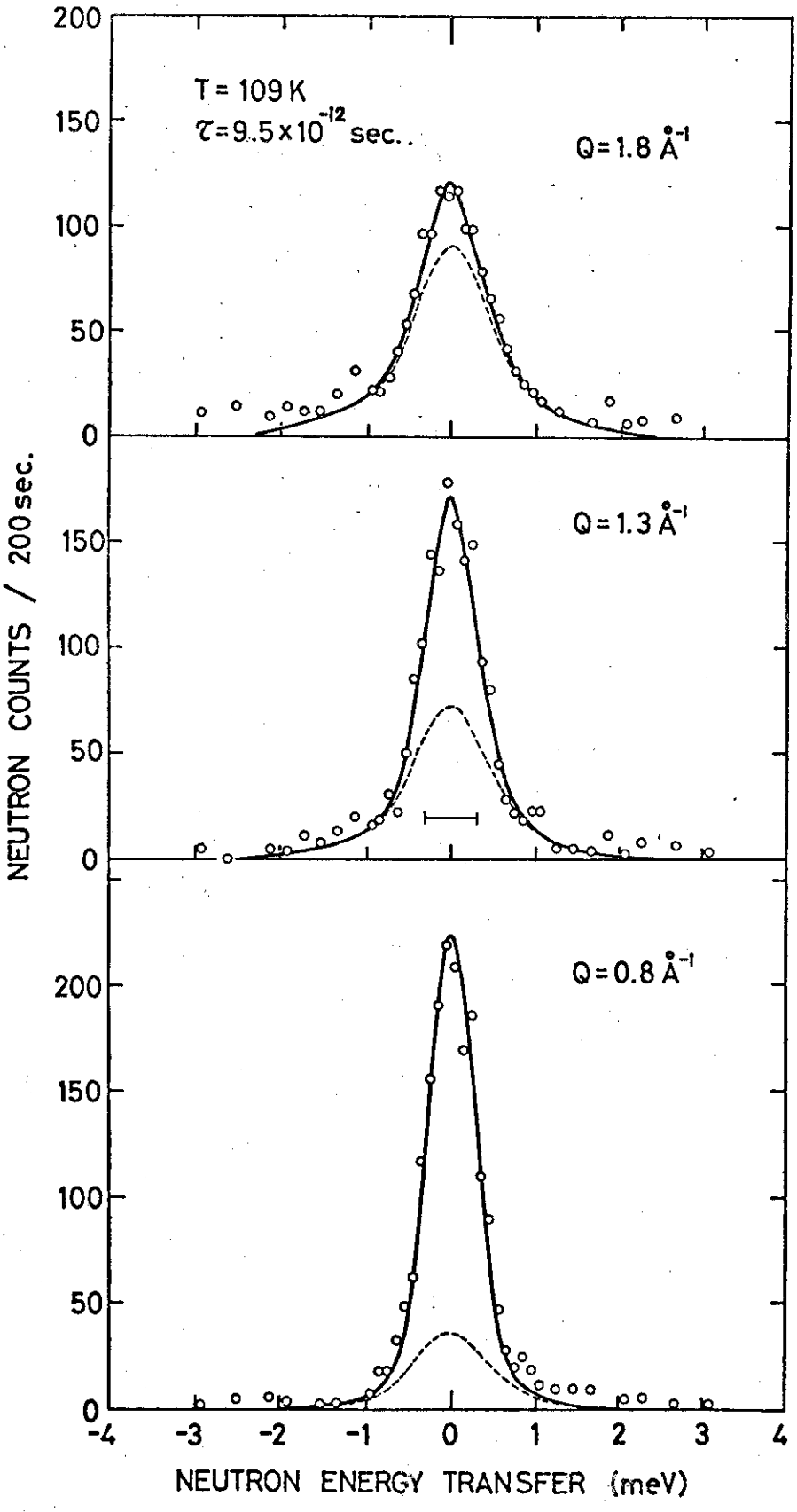
T = 109 K
τ = 9.5 x 10^-12 sec.
Q = 1.8 Å^-1
Q = 1.3 Å^-1
Q = 0.8 Å^-1
NEUTRON COUNTS / 200 sec.
NEUTRON ENERGY TRANSFER (meV)

Fig. 1

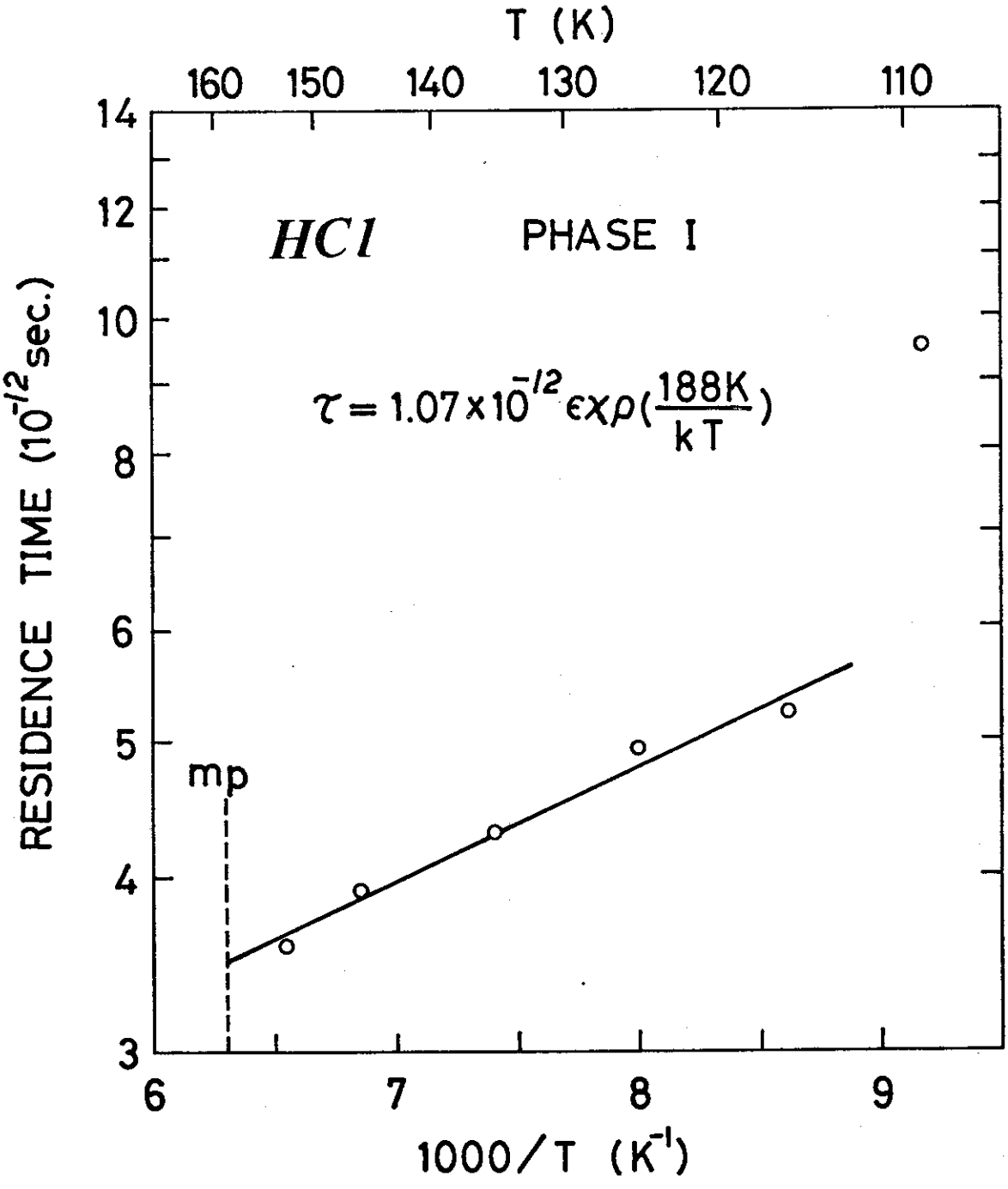
T (K)
160
150
140
130
120
110
14
12
10
8
6
5
4
3
HCl
PHASE I
$\tau = 1.07 \times 10^{-12} \exp(\frac{188K}{kT})$
mp
RESIDENCE TIME (10^{-12}sec.)
6
7
8
9
1000/T (K^{-1})

Fig. 2

Helical Magnetic Structure in CrB_2

by Satoru FUNAHASHI, Yoshikazu HAMAGUCHI, Takaho TANAKA* and Eisuke BANNAI* (Physics Division, JAERI; *National Institute for Researches in Inorganic Materials)

CrB_2 is a hexagonal (P6/mmm) metallic compound which has the T_N about 86K. Chromium-like magnetism was presupposed by Barnes et al.[1] from the nmr behaviors of ^{11}B. Liu et al.[2] predicted the SDW which propagates along the c-axis from the energy band calculation.

We measured the magnetic neutron diffraction with the spectrometer CTNS of a single crystal prepared with natural boron. We used a very thin sample ($0.23\times7\times30mm^3$) to optimize the diffraction intensity. Satellite reflections were found below the T_N on the (110)-axis with $\vec{\tau}=0.285\vec{\tau}_{110}$. Here $\vec{\tau}_{110}$ is the reciprocal lattice vector of 110. Satellites were also observed at the crystallographically equivalent positions as illustrated in Fig.1, while any superfluous reflections were not detected either on the (001)-axis or on the (100)-axis. The intensity of the fundamental reflections does not change through the T_N. Therefore, the simple incommensurate magnetic structures, i.e. the SDW and the helical structure were examined to explain the satellite intensity shown in Fig.2. Each structure is classified into three cases according to the magnetic anisotropy. The cycloidal structure illustrated in Fig.3 best fits the intensity among them. The magnetic moment is $0.5\pm0.1\mu_B$. The details have been published in reference 3).

REFERENCES

1) R.G.Barnes & R.B.Creel, Physics Letters 29A(1969)203.

2) S.H.Liu, L.Kopp, W.B.England & H.W.Myron, Phys.Rev. B11(1975)3463.

3) S.Funahashi, Y.Hamaguchi, T.Tanaka & E.Bannai, Solid State Commun. 23(1977)859.

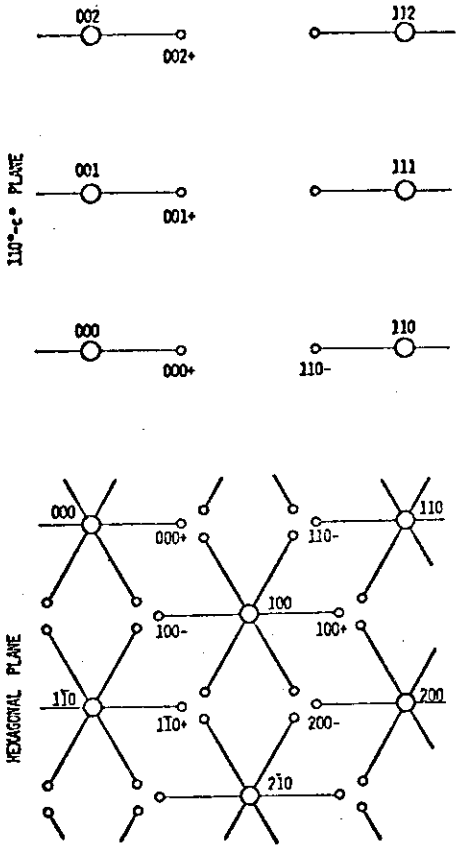

Fig.1 Satellite reflection positions in the reciprocal lattice space.

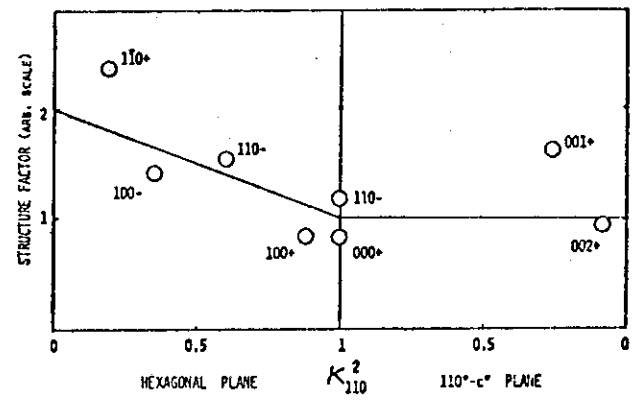

Fig.2 Satellite reflection intensity as a function of K_{110}^2. K_{110} is the direction cosine of the scattering vector with respect to τ_{110}. Form factor is assumed to be same as pure Cr. Solid line represents the structure factor of the cycloidal structure illustrated in Fig.3.

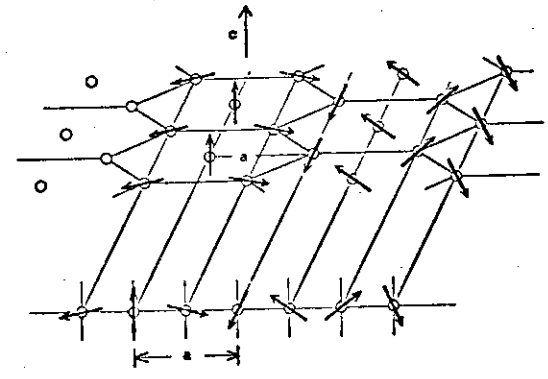

Fig.3 Schematic picture of the cycloidal structure of CrB_2. Projection of the spins on a-c plane is also shown.

Single Crystal Neutron Diffraction Study of $SrFeO_{3-x}$ (x=0.1)

by Hitoshi Oda, Yasuo Yamaguchi, Humihiko Takei and Hiroshi Watanabe

(The Research Institute for Iron, Steel and Other Metals, Tohoku University)

Perovskite-type oxide $SrFeO_3$ contains Fe^{4+} ion ($3d^4$) and shows metallic conductivity with $\rho \sim 10^{-3}\Omega\cdot$cm. It has a peoper screw spin structure with the propagation vector parallel to a [111] direction below the Néel temperature of 134K. We have synthesized the single crystals of $SrFeO_{3-x}$ (x=0.1) and carried out the neutron diffraction study.

In Fig. 1, it showed the temperature dependence of the magnetic moment which was obtained from the intensity of the satellite (δ, δ,δ). In Fig. 2, the temperature dependence of the propagation vector was shown, which was evaluated from the peak position of (δ, δ, δ). The absolute value of the propagation vector is almost constant, $0.130\times\sqrt{3}\cdot 2\pi/a$ $\mathring{A}^{-1}$, at temperature below 50K, while it decreases gradually at higher temperatures reaching to $0.118\times\sqrt{3}\cdot 2\pi/a$ $\mathring{A}^{-1}$ at T_N.

The magnetic form factor per unit cell was obtained at 4.2K from the intensities of the satellites for $\sin\theta/\lambda$ smaller than 0.4 $\mathring{A}^{-1}$ as shown in Fig. 3. The magnetic moment of Fe^{4+} ion was about 2.3 μ_B evaluated by using the spherical form factor of Fe^{4+} ion, thus Fe^{4+} ion ($3d^4$) was close to the low-spin state (t_{2g}^4). The deviation of the observed form factor from the calculated one should be explained with the magnetic moment of 0.3 μ_B on the oxygen ion which was antiparallel to the vector sum of the magnetic moments of two iron

ions lying on the neighbouring planes perpendicular to the screw axis.

The magnetic polarization on the oxygen ion seemed to be due to the strong covalent bonding of O^{2-}-Fe^{4+}, especially the covalency effect of the hybrid p_σ-e_g orbitals.

This work has been published in J. Phys. Soc. Japan. 42 (1977) 101.

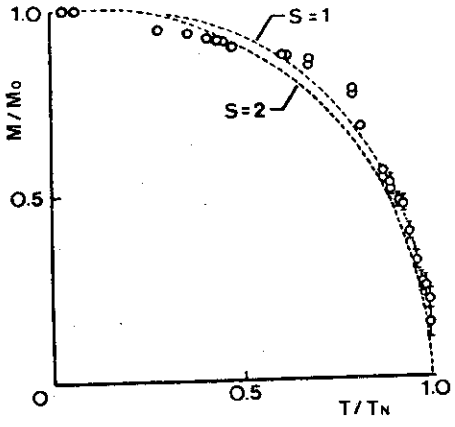

Fig. 1

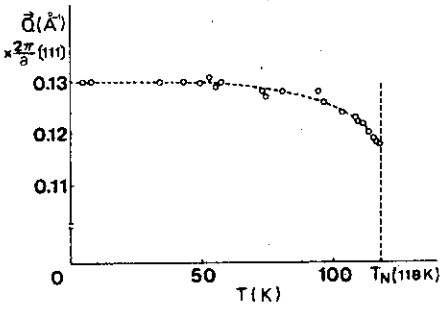

Fig. 2

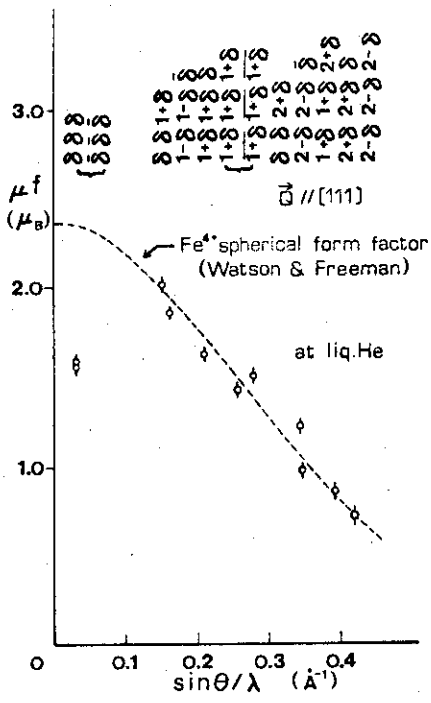

Fig. 3

Fig. 1. Temperature dependence of the magnetic moment. The broken curves indicate Brillouin function with spin 1 and 2.

Fig. 2. Temperature dependence of the propagation vector.

Fig. 3. Magnetic form factor at liq.He temperature. The broken curve is the spherical form factor of Fe^{4+} ion calculated by Watson and Freeman.

Polarized Neutron Diffraction Study of $CuCr_2Se_4$ Single Crystal

by Osamu Yamashita, Yasuo Yamaguchi, Isao Nakatani[+],
Hiroshi Watanabe and Katashi Masumoto[+]
(The Research Institute for Iron, Steel and Other Metals,
Tohoku University)
([+]National Research Institute for Metals)

The series of chromium chalcogenides ACr_2X_4 (S=Cu, Cd, Hg, X= S, Se, Te) with the normal spinel structure have been studied in detail on the magnetic properties and electric resistivities.[1-3] The materials ACr_2X_4 with A=Cd, Hg, are all semiconductive ferromagnets with the magnetic moments near 6.0 μ_B per formula which is reasonably understandable for the t_{2g}^3 (S=3/2) electron configuration of Cr^{3+} ions in octahedral sites. The paramagnetic Curie constants observed are also explained well with this configuration. Therefore, in these materials chromium atoms are considered to be in the Cr^{3+} state, and the substance can be described well with the localized electron picture.

On the other hand the compounds $CuCr_2X_4$ with X=S, Se and Te are metallic ferromagnets with the magnetic moment of about 5.0 μ_B per formula, so that these compounds may not be treated simply as ionic crystals. Furthermore these materials have an interesting character showing relatively high Curie temperatures (Tc=432K in $CuCr_2Se_4$) as compared with those of semiconductive spinels (e.g. Tc=130K for $CdCr_2Se_4$). This fact would indicate that the carrier responsible for metallic conduction causes strong stabilization of the ferromagnetic state in $CuCr_2X_4$ (X=S, Se, Te). We chose $CuCr_2Se_4$ as a typical example of these metallic ferromagnets, and studied its electronic

state by means of the polarized neutron diffraction technique. From the measured form factor of copper and chromium atoms, the magnetic moments are determined to be -0.07±0.02 (μ_B/Cu) and 2.64±0.04 (μ_B/Cr), respectively. Further the uniform polarization existent throughout the crystal is estimated to be -0.20±0.11 μ_B per formula, using the total moment 5.01±0.01 (μ_B/ $CuCr_2Se_4$) obtained from the magnetization measurement. This result which differs from those reported by other authors with neutron diffraction, shows that neither of the ionic configuration models of $Cu^+[Cr^{3+}Cr^{4+}]Se_4$ nor $Cu^{2+}[Cr_2{}^{3+}]Se_4$ gives a satisfactory explanation of $CuCr_2Se_4$, although the former is closer to the experimental data. The form factor of the chromium atom agrees well with the calculated free ion form factor for V^{2+}, but not for Cr^{3+}, and this fact indicates that the unpaired electron density on the chromium atom is more spread than that for free Cr^{3+}. It is found that 79±6% of the unpaired 3d electrons occupy t_{2g} orbitals.

The presence of magnetic moments on all constituent atoms means that the Fermi level lies below the top of the bands composed of Cu t_{2g}, Se 4p and Cr t_{2g} orbitals, so as to produce p-type conduction. As was stated, this material shows a relatively high Curie temperature as compared with those of other semiconductive spinels, in which the ferromagnetic mechanism is mainly right angle superexchange interaction. On the contrary in $CuCr_2Se_4$, apart from the above mechanism, 3d-holes in t_{2g} band which contribute to the conduction, contribute as well to ferromagnetism through both direct coupling and indirect coupling via holes in the valence band.

This work will be published in J.Phys. Soc. Japan.

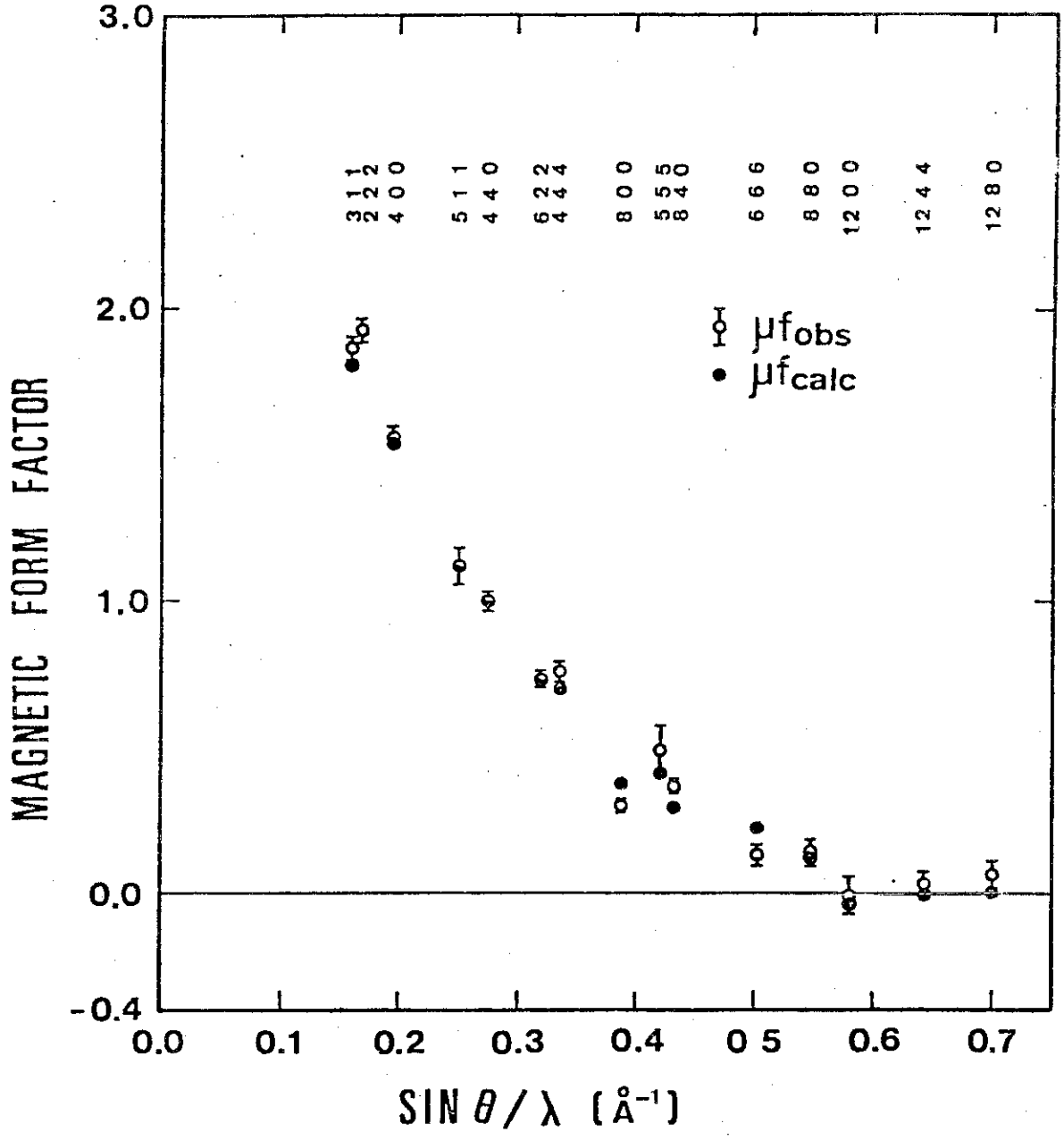

Fig. 1 Comparison between measured and calculated magnetic form factors.

Incommensurate Spin Density Wave State under High Pressure in 3.7%Fe-Cr Alloy

by Jun'ichiro Mizuki, Yasuo Endoh, and Yoshikazu Ishikawa
(Department of Physics, Tohoku University)

Dilute FeCr alloys are important classes to understand the effect of magnetic impurities on the itinerant antiferromagnetism. Because a magnetic phase diagram of these alloys is quite different from those of other alloy systems, such as Cr-Mn, or Cr-V. Fe forms a localized magnetic moment and others do not. Also the pressure effect is not similar, which turns out that the role of the localized magnetic moment is quite different from that of itinerant electrons. Theoretical studies on this matter suggested the importance of the enhancement of the magnetostrictine forces in the presence of such magnetic impurities. Thus the change of SDW state with applying pressure is very interesting. In experimental side of view, we must find out the origin of the significant descrepancy in the phase diagram of FeCr at the atmospheric pressure. One found the coexistence of both incommensurate and commensurate state and others did not in the same composition. This is not owing to the measuring techniques but owing to samples, in other words, the different techniques preparing samples for measurements. If the internal pressure exists by the presence of other defects than magnetic impurities, the pressure dependence, $\partial\eta/\partial p$, where η is a physical order parameter, can be unique.

Neutron diffraction studies under pressure up to $\sim$5 k bar were carried out using a pressure cell in which a 3.7% Fe-Cr

single crystal with CS_2 as the pressure transformer were clamped at high pressure. This method has large advantage of ease of handling, but sucrifies the isobar condition at various temperatures.

Although we found some technical difficulties which must be overcome, the pressure effect was very clear in the way what was expected. So far we have obtained a preliminary phase diagram in (P,T) plane by the measuring of both the (0,0,1) magnetic reflection and the (0,0,1±δ) satellites at different temperatures (T) and pressure (P).

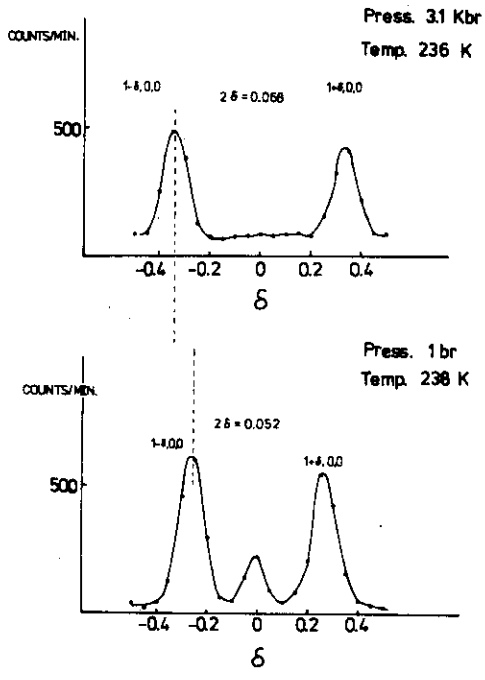

Fig[1]

Diffraction patterns of 3.7% FeCr alloy at 0 and 5 kbar. Pressure was calibrated by using the change of the lattice parameter of KCl and compressibility. These measurements were done separately.

Strain Wave in Chromium Alloys

Satoshi IIDA, Masaharu KOHNO,* Yorihiko TSUNODA,
Nobuhiko KUNITOMI
Faculty of Science, Osaka University, Toyonaka
Osaka, 560

Recent neutron diffraction measurements by Pynn et al[1] has indicated that, in pure Cr, strain wave (SD) amplitude Δ_{2Q} is proportional to the square of $\langle\mu_Q\rangle$, the amplitude of the spin density wave (SDW), when $\langle\mu_Q\rangle$ is varied as a function of temperature. In the present investigation, the relation between Δ_{2Q} and $\langle\mu_Q\rangle$ was studied when $\langle\mu_Q\rangle$ is varied by adding proper amounts of impurities in Cr. For this purpose, amplitudes of SW and SDW were determined by neutron diffraction for dilute Cr based CrMn and CrV alloys.

The specimens used were single crystals cut out from ingots arc-melted in an argon atmosphere.

The scattering intensities of nuclear Bragg, SDW satellite and SW satellite reflections are expressed as

$$I_{N.B.}=N\frac{(2\pi)^3}{V0}(\bar{b})^2\sum_{\tau}\delta(\kappa-\tau)\frac{1}{\sin 2\theta}$$

$$I_{SDW}=N\frac{(2\pi)^3}{V0}\left\{\frac{\gamma e^2}{mc2}Sf(\kappa)\right\}^2\sum_{\tau}\delta(\kappa-\tau\pm Q)\frac{1}{\sin 2\theta}\{1-(\hat{\tau}\cdot\hat{\eta})\}_{AV}$$

$$I_{SW}=N\frac{(2\pi)^3}{V_0}(\bar{b})^2\frac{\{(\kappa\cdot\Delta_{2Q})^2\}}{4}AV\frac{1}{SIN2\theta}\sum_{\tau}\delta(\kappa-\tau\pm 2Q)$$

respectively.

By means of X-ray diffraction, we can observe the ratio of I_{SW} and I_{NB}, but it is necessary to have full knowledge of magnetic domain distributions in order to determine Δ_{2Q} from I_{SW}. Recalling that the same magnetic domain contributes to I_{SDW} and I_{SW}, we observed I_{SW}/I_{SDW} by neutron diffraction which enabled us to evaluate $\Delta_{2Q}/\langle\mu_Q\rangle$ without the knowledge of the domain distributions. By such a method, we can

---

*Present adress; Kobe Steel Ltd.Wakihamacho,Fukiaiku, Kobe, 651

avoid the difficulty due to the extinction effect which is inevitable if we observe rather strong nuclear reflection.

In fig. 1, $\sqrt{I_{SW}/I_{SDW}}$, which is proportional to $\Delta_{2Q}/\langle\mu_Q\rangle$, are plotted as a function of $\langle\mu_Q\rangle$ for several specimens, where $\langle\mu_Q\rangle$ for each sample was estimated by using the reported data of T_N, SDW wave number Q, $\langle\mu_Q\rangle$ and the relation between them by Koehler et al[2]. From fig. 1, we may say that Δ_{2Q} is again proportional to $\langle\mu_Q\rangle^2$ when $\langle\mu_Q\rangle$ is varied by alloying effect.

We intend to study the temperature dependence of Δ_{2Q} and $\langle\mu_Q\rangle$ by X-ray and neutron diffractions and to compare the contribution to the SW amplitude by the alloying and the temperature varying effects.

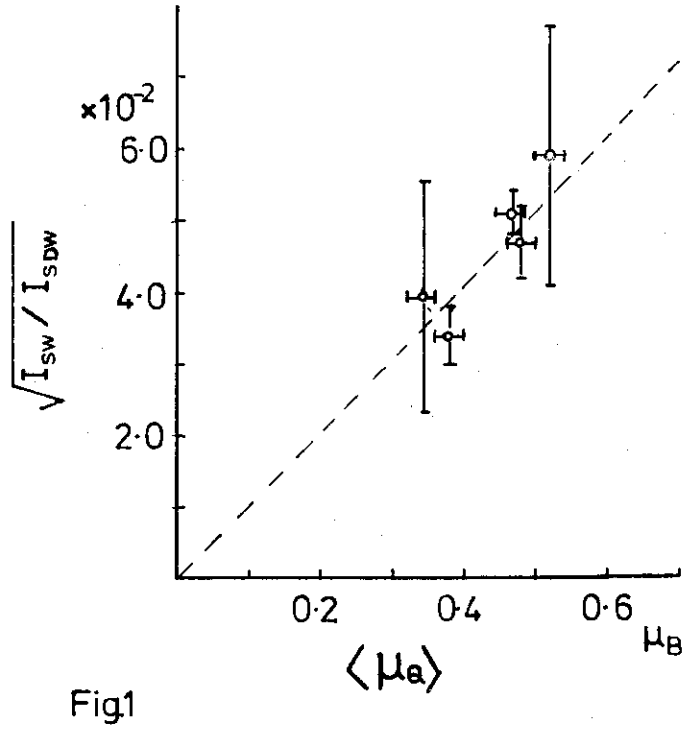

Fig.1

(1) R. Pynn, W. Press, S.M. Shapiro, S.A. Werner Phys. Rev. B13(1976)295

(2) W.C. Koehler, R.M. Moon, A.L. Trego, A.R. Mackintosh Phys. Rev. 151(1966)405

Electronic State of Low Spin MnAs(P)

by Satoshi Haneda, Noriaki Kazama, Yasuo Yamaguchi and Hiroshi Watanabe

(The Research Institute for Iron, Steel and Other Metals, Tohoku University)

The compound MnAs is in the high spin state all over the temperature range, while the compounds with As partially substituted by P and MnAs under high pressure are apt to be stabilized by taking the low spin state. We have reconfirmed this fact through an investigation of the electronic state by the magnetic form factor measurement. (The effect of the substitution of P for As is almost equivalent to the pressure effect.)

We carried out neutron diffraction measurement with a single crystal $MnAs_{1-x}P_x$(x=0.075) (2mmϕ×3mm) in order to determine the magnetic form factor, with the expectation that the electronic state would be clarified. The knowledge of the electronic state may explain some anomalous changes of the physical properties.

The magnetic structure and the magnetic form factor of low spin state MnAs(P) were determined at 78K from neutron diffraction, and some interesting results were obtained by analyzing the form factor and comparing them with those of high spin MnAs. (i) The magnetic structure is a double spiral structure with the propagation vector $q=0.111\times a^*$, the phase angle $\alpha(\phi_2-\phi_1)=31^\circ$ and the magnetic moment $2S=1.80\pm0.05$ at 78K. (ii) Electron configuration was determined from the asphericity of the magnetic form factors. By using a similar method to that for MnAs, the electron configuration determined is $(1\uparrow+1\downarrow,\ 2\uparrow,\ 0)$ for $(\psi_{x0},\ \psi_{x\pm},\ \psi_{u\pm})$ orbitals. (iii) The spherical

form factor of the high spin state spreads more than that of the low spin state. This would be due to the change of covalency. (High spin-low spin transition is accompanied by a large change of the lattice volume.) (iv) Corresponding to this lattice contraction it is known that the electical resistivity increases. This phenomenon can be explained qualitatively by the change of the 3d electron configuration.

This work has been published in J. Phys. Soc. Japan 42 (1977) 1212.

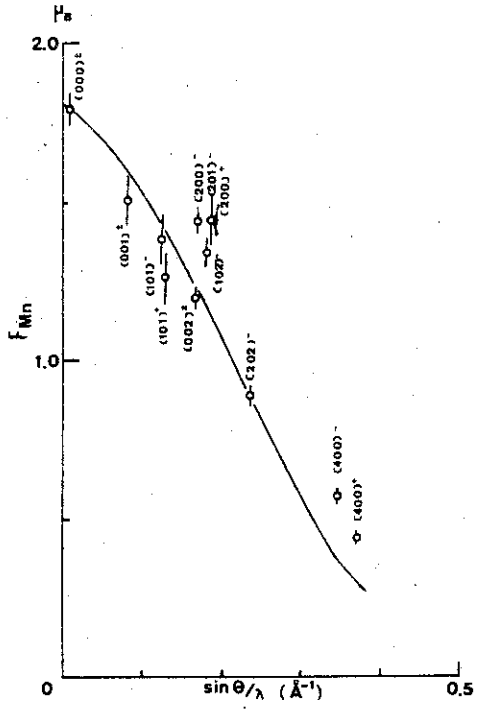

Fig. 1. Magnetic form factors in the case of $\alpha=31^{\circ}$. Large asphericity is observed, which represents the anisotropic unpaired electron distribution. Errors are ditermined from the reliability factor R. The solid line indicates the spherical form factor.

Electronic State of High Spin MnAs

by Satoshi Haneda, Noriaki Kazama, Yasuo Yamaguchi and Hiroshi Watanabe

(The Research Institute for Iron, Steel and Other Metals, Tohoku University)

MnAs is a typical ferromagnetic compound of NiAs type and undergoes a very interesting high spin-low spin transition. Thus MnAs is in a critical region of a high spin state which is easily transformed to a low spin state by hydrostatic pressure or substitution of P for As. These results indicate that 3d electrons in an Mn atom are exposed to the strong ligand field created by strong covalency with ligands. Therefore MnAs shows some deviations from ionic character that the electrical resistivity is metallic, viz., 2×10^{-4} $\Omega\cdot$cm at room temperature, and the magnetic moment per Mn atom takes a non-integer value of 3.4 μ_B at 4.2K. If an As atom takes As^{3-} ionic state, which has $4s^2 4p^6$ electrons, the ionic state of Mn should be Mn^{3+}, which has magnetic moment of 4 μ_B in the perfectly high spin state. The measurement of the magnetic structure factors is expected to give a clear understanding for all of these experimental results.

The magnetic form factor of high spin MnAs was investigated by using the polarized neutron technique. The experimental results (Fig. 1) were compared with calculation, and we got some conclusion on the electronic state of high spin MnAs: i) By analyzing the asphericity of the magnetic form factor with the free ion model, the numbers of electrons in the atomic levels were determined to be $(1.0\uparrow+0.3\downarrow,\ 2.0\uparrow,\ 0.7\uparrow)$ for $(\Psi_{x0},\ \Psi_{x\pm},\ \Psi_{u\pm})$ atomic levels,

respectively. Therefore, Mn atoms are in the $3d^4$ electronic state in MnAs. ii) This electron configuration is convenient to explain the observed metallic conductivity. iii) The spin density distribution, which is the Fourier transformation of magnetic form factor, shows the characteristics of the above mentioned electron configuration and the strong covalency with the anion As as shown in Fig. 2. iv) Spherical part of the magnetic form factor agrees with the calculated one for Mn^+, not for Mn^{3+}. But this does not imply the Mn atoms is in the Mn^+ state.

This work has been published in J. Phys. Soc. Japan. 42 (1977) 1201.

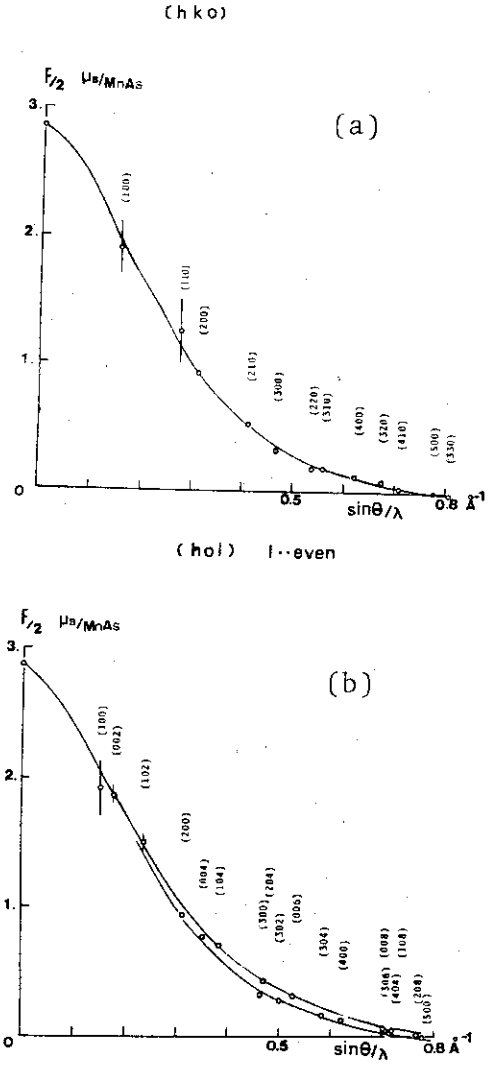

Fig. 1. Observed magnetic form factors of (a) (hko) and (b) (hol) reflections at 293K.

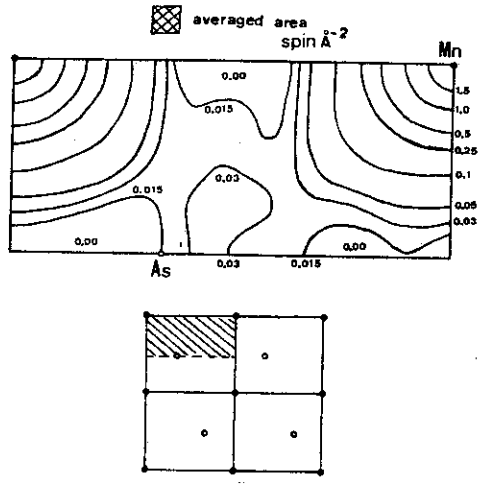

Fig. 2. Spin density map peojected on a-plane. It corresponds to the shaded part of the figure shown below.

High Spin-Low Spin Transition in $MnAs_{1-x}P_x$ (x=0.075)

by Satoshi Naneda, Noriaki Kazama, Yasuo Yamaguchi and Hiroshi Watanabe

(The Research Institute for Iron, Steel and Other Metals, Tohoku University)

The compounds $MnAs_{1-x}P_x$ with $x \geq 0.03$ show very interesting magnetic properties. Goodenough et al. and Ido studied these properties in relation to crystal structure.[1-3] These authors showed from magnetic and X-ray diffraction measurements that there are three transition temperatures T_1, T_2 and T_N for these compounds. Above T_2, these compounds have the hexagonal NiAs structure ($B8_1$), and transform to the orthorhombic MnP structure (B31) below T_2. The temperature T_1 is defined as the bending point of the inverse susceptibility vs temperature curve between T_2 and the Néel temperature T_N. Goodenough et al. pointed out that the high spin-low spin transition takes place in the interval between T_2 and T_1. But Hall et al.[4] reported from neutron diffraction on the powdered sample that $MnAs_{0.92}P_{0.08}$ is canted ferromagnetic at low temperature and it is in the high spin state all over the temperature range.

In the present study, magnetic reflections were observed at the scattering angle corresponding to the reflection (001) and on both sides of (101). Hall et al.[4] could not resolve the magnetic reflection from the nuclear reflection around (101). We analyzed the magnetic reflections on a model with a single magnetic mode and the magnetic reflections were indexed as $(001)^{\pm}$ and $(101)^{\pm}$. The relative intensities were analyzed by assuming Mn^{3+} magnetic form factor calculated by Watson and Freeman.[6] A double spiral spin structure

shown in Fig. 2 was established with the magnetic moment of $\mu=2.0\pm 0.4\ \mu_B/Mn$ which corresponds to the low spin state of Mn^{3+} and the propagation vector of $q=(0.10\pm 0.01)\times a^*$. This spin structure was reconfirmed by the experiment on a single crystal.[5)]

In this time, some of the physical properties of the compound $MnAs_{1-x}P_x$(x=0.075) are also investigated by the various measurements, and they can be divided into four different temperature ranges. The compound is: i) for $T>T_2$(=430K), a high spin state paramagnet with the NiAs type ($B8_1$), ii) for T_1(≃315K) $T<T_2$, a high spin state paramagnet with the MnP type (B31), iii) for T_N(=232K)$<T<T_1$, an intermediate spin state paramagnet with the MnP type and iv) for $T<T_N$, a low spin state antiferromagnet with the MnP type. Especially in the region iii), an interesting phenomenon of a high spin-low spin transition is observed, and characterized by a large change in the lattice constants and the electrical resistivity.

This work has been published in J. Phys. Soc. Japan 42 (1977) 31.

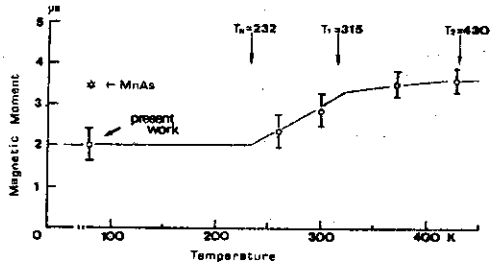

Fig. 1. Temperature dependence of the localized magnetic moment. The values above T_N are the results by L.H. Schwartz et al.

Magnetic Moment of Excess Mn in $Mn_{1+\delta}Sb$

by Yasuo Yamaguchi, Hiroshi Watanabe and Takashi Suzuki
(The Research Institute for Iron, Steel and Other Metals,
Tohoku University)

Recently, NiAs type ferromagnets MnSb and MnBi have been studied in detail with the single crystal specimens and it was pointed out that the excess Mn atoms have large effects on the magnetic and electrical properties of these materials. The intermetallic compound $Mn_{1+\delta}Sb$ takes NiAs crystal structure through a wide composition range with $0 \leq \delta \leq 0.22$. The spontaneous magnetization and also the Curie temperature of $Mn_{1+\delta}Sb$ decrease linearly with increase of δ;i.e.

$\mu = (3.57-2.78\times\delta)\mu_B$/formula at 4.2K,

and $Tc=(577-790\times\delta)K$.

From the above μ vs δ relation, the excess Mn moments are considered to be directed antiparallel to the total magnetization. The magnetic susceptibility measurements, however, show that the Curie constants of $Mn_{1+\delta}Sb$ cannot be analyzed with the simple picture of the antiparallel alignment of the excess Mn moments.

In the present investigation, the magnetic moments of the excess Mn atoms are studied by using the polarized neutron diffraction (PND) technique, which is well known as a very powerful means to observe a small magnetization in the crystals. The excess Mn atoms occupy the interstitial sites of NiAs structure, so that there is a difference in the symmetry between regular and excess Mn sites. This fact enable us to observe the small amount of magnetization on the excess Mn atoms by measuring the "forbidden" reflections for regular site Mn atoms, i.e. (hkl) reflections with l odd for NiAs structure.

In the present investigation, $Mn_{1.05}Sb$ and $Mn_{1.18}Sb$ were studied, and the result is shown in Fig. 1. One can see in Fig. 1 that the contribution of the excess Mn atoms is confined to the low angle reflections, especially only to the (101) reflection. If an excess Mn atom has a local magnetic moment, it must be due to the 3d-electron polarization, and then the difference in the magnetic structure factors between $Mn_{1.05}Sb$ and $Mn_{1.18}Sb$ should have the shape of the magnetic form factor of Mn 3d-electrons as shown in Fig. 1 with the solid lines. Therefore, one can conclude that the excess Mn atoms have no 3d-electron polarization within the experimental error.

In conclusion, the excess Mn atoms have no magnetic moment, but affect the regular site Mn atoms to decrease the magnetization. This work has been published in J. Phys. Soc. Japan. 41 (1976) 703.

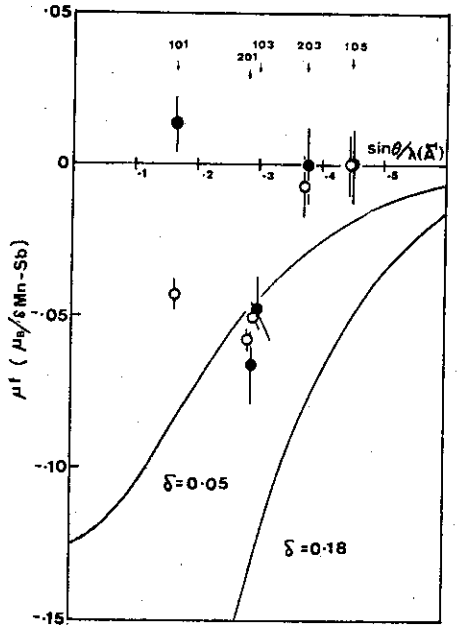

Fig. 1. Magnetic form factors of $Mn_{1+\delta}Sb$ per δ part of excess Mn, in unit of the Bohr magneton, for reflections with l odd. Comparison between the observations for $Mn_{1.05}Sb$( ) and $Mn_{1.18}Sb$( ) at 293K. Solid curves give the calculated values by assuming -2.78 μ_B per excess Mn atom.

Atomic Magnetic Moments in Fe-V Alloys

by Osamu Yamashita, Yasuo Yamaguchi and Hiroshi Watanabe
(The Research Institute for Iron, Steel and Other Metals,
Tohoku University)

Polarized neutron diffraction measurements were made on a series of ferromagnetic Fe-V alloys in order to determine the atomic magnetic moments in this alloy system.

The average atomic magnetic moments of ferromagnetic transition metal alloys are represented by Slater-Pauling curve. In Fe-Cr and Fe-V alloys with bcc structure, the average moments decrease linearly with increasing of Cr and V contents, respectively. The magnetic moments in Fe-Cr alloys are in excellent agreement with the calculated values based on CPA theory. This approximation requires that constituent elements are near neighbour in periodic table.

In Fe-V alloy which Fe and V elements are third neighbour in periodic table, we are interested in whether CPA theory can be applied for the estimation of the individual magnetic moments in Fe-V alloys.

The values of the individual Fe and V moments were determined from both the diffuse and Bragg scattering as shown in Fig. 1. The magnetic moment on an Fe atom remains unaffected by alloying below about 30 at.%V, while it decreases rapidly with increasing V content above that value. On the other hand, the magnetic moment on a V atom is negative for low V concentrations and approaches zero near about 30 at.%V. These experimental results are qualitatively similar to those of Fe-Cr alloys observed by Shull and Wilkinson.
This work will be published in J. Phys. Soc. Japan.

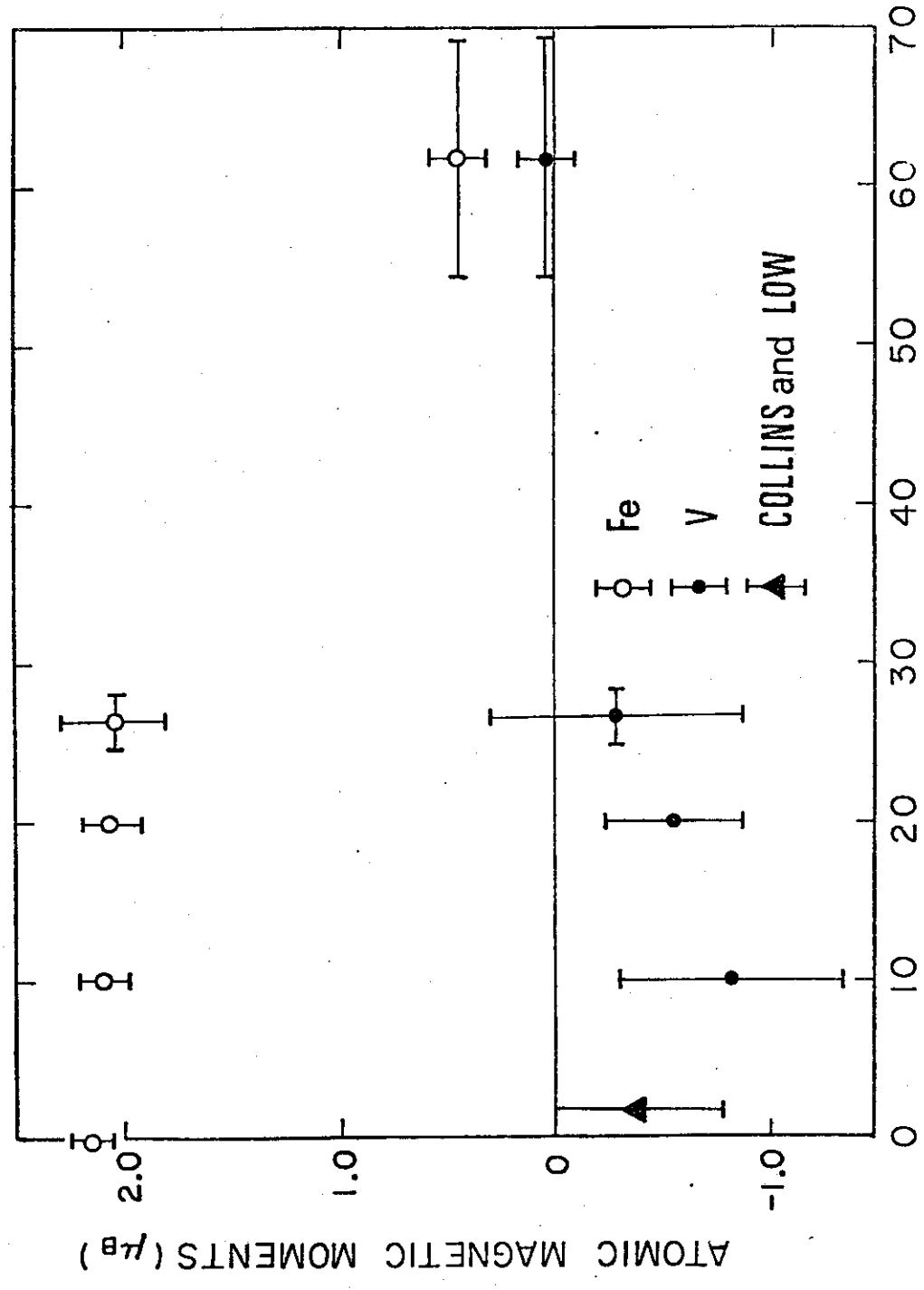
ATOMIC MAGNETIC MOMENTS (μ_B)
2.0
1.0
0
-1.0
0
10
20
30
40
50
60
70
AT.% V
Fe
V
COLLINS and LOW

Fig. 1

Average Magnetic Moment of Mn Impurity in Ferromagnetic Ni-Co Alloy

Yoshihiro SHIOZAKI, Yutaka NAKAI, Nobuhiko KUNITOMI
Faculty of Science, Osaka University, Toyonaka
Osaka, 560

1. Introduction The magnetic moment of a constituent atom in an alloy is strongly dependent on the atomic concentration on its nearest neighbouring shell (enviroment effect). Since Mn moment couples ferromagnetically with Ni moment and antiferromanetically with Co, Mn impurity in Ni-Co alloys may have parallel or antiparallel polarization wity respect to the bulk magnetization according to its enveroment and its average moment may change its sign at the critical alloy composition.

We have measured this change of the mean Mn moment by means of diffuse scattering of polarized neutrons and compared it with the results of extened-CPA theory.(1)

2. Measurements Nine specimens of NiCo(Mn) containing from 0.0 to 60.0 at.%Co and 2.0 at.%Mn were prepared by arc-melting the proper amounts of Ni, Co and Mn having 3N in purity. Typical dimension of specimens was of 30 x 20 x 2 mm rectangular plate.

Polarized neutron diffuse scattering measurements were performed by POLTO diffractometer at room temperature. The applied magnetic field was about 10 kOe. The absolute value of cross sections were obtained by calibrating the observed intensities with those of standard NH_4Cl and vanadium plates.

By measuring the cross sections of parallel and antiparallel polarization of neutrons, we have obtained the nuclear and magnetic interference term which consists of three contributions; Ni-Co, Ni-Mn and Co-Mn pair cross terms. Fortunately, for Ni-Co alloys it has been known that the atomic ordering effect is negligibly small and the magnetic moment of Ni and Co in alloys is nearly constant for all alloy compositions and Mn has negative scattering length. Assuming that Ni and Co moments are constant for all specimens, we can extract the Mn contributions. Multiple Bragg scattering were corrected by a computer simulation method (Fig.1).

After these corrections and assumptions, averaged Mn magnetic moments are determined and listed in Table I; the dependence on alloy compositions are shown in Fig. 2.

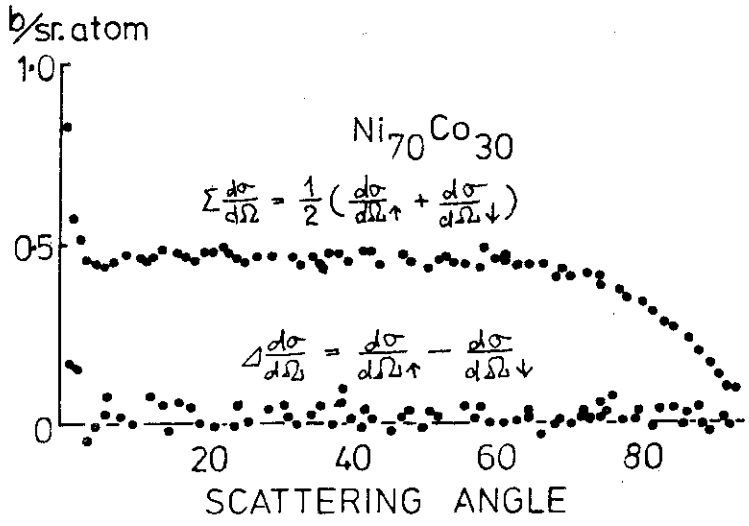

Figure 1
The computer simulation of multiple Bragg scattering: The difference cross section was used to correct the data.

3. Results The dashed curve in Fig.2 shows the theoretical expectation from the extended-CPA calculations. The apparent discrepancy between the theoretical and experimental results is probably brought about by temperature effect neglected in the theoretical calculation. Parallel state of Mn moment is supposed to be unstable against the temperature agitation as observed in Ni-Mn and Fe-Mn alloys.[2),(3)] It is necessary to measure the present specimens at low temperature, and it is interesting to study the thermal localized fluctuation of Mn moment in ferromagnetic Ni-Co alloy by, for example, electrical resistivity measurements.

We are preparing to perform the experiments of polarized neutron

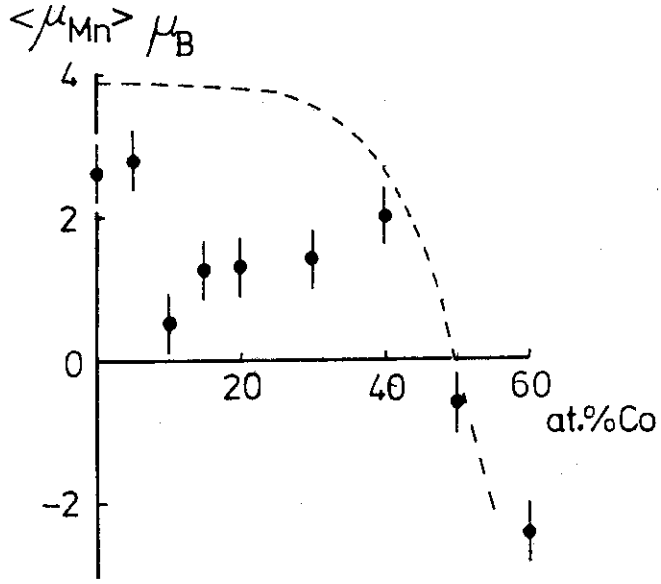

Figure 2
Co-concentration dependence of average Mn moment: The dashed curve is theoretical expectation for absolute zero temperature. Experimental results were obtained at room temperature.

Table I

at.%Co	$< \mu_{Mn} >$	at.%Co	$< \mu_{Mn} >$
0	2.61 ± 0.45	30	1.41 ± 0.25
5	2.80 ± 0.40	40	1.99 ± 0.43
10	0.47 ± 0.47	50	-0.59 ± 0.42
15	1.27 ± 0.32	60	-2.42 ± 0.46
20	1.32 ± 0.37		

Mn moment in Bohr magneton

scattering at low temperature.

References

(1) T. Jo Thesis 1975, Faculty of Science, Osaka University

(2) J.W. Cable and H.R. Child Phys. Rev. B10 (1974) 4607

(3) Y. Nakai and N. Kunitomi J. Phys. Soc. Japan 39 (1975) 1257

Magnetic Moment Distributions for Ferromagnetic Co-Mn Alloys

— Existence of Two Magnetic States in Mn Atoms —

Yutaka NAKAI, Kazuo HOZAKI*, Nobuhiko KUNITOMI
Faculty of Science, Osaka University, Toyonaka
Osaka, 560

The magnetic moment distributions in f.c.c. Co-Mn alloys has been determined by means of diffuse scattering of unpolarized and polarized neutrons. Four specimens containing from 7.6 to 25.0 at.% Mn were prepared by argon arc-melting the requisite amounts of 99.9% Co and 99.99% Mn. After shaped into rectangular plates of 27 x 20 x 2 mm, these were annealed at 700°C for 3 hours and quenched into water in order to stabilize f.c.c. phase.

Neutron diffuse scattering measurements were made by TOG and POLTO neutron diffractometers, each of which was used for the unpolarized and polarized neutron scattering measurement, respectively. The absolute value of cross sections were determined by calibrating the observed intensity with that for a standard specimen of a V plate with the thickness of 2mm. The measurements were made at room temperature and at 98°K. The magnetic field applied in order to eliminate the magnetic contribution were about 10 and 6.5 KOe for polarized and unpolarized neutron experiments, respectively.

(i) Polarized neutron experiment

By measuring the cross sections for parallel and antiparallel polarizations of neutrons and by taking their difference, the interference term of the nuclear and magnetic scattering can be extracted. The difference cross section is expressed as

$$\Delta\frac{d\sigma}{d\Omega} = 1.079\ c\ (1-c)\ (b_{Co} - b_{Mn})[\ \langle\mu_{Co}\rangle - \langle\mu_{Mn}\rangle\ ], \quad (1)$$

if small oscillatory term due to the moment fluctuation is ignored. In this equation, $\langle\mu_i\rangle$ denotes configuration average of K-dependent magnetic moment of atomic specie i and other notations follow the common use. From the observed values of cross sections average magne-

---

* Present adress: Sumitomo Metal Industries LTD. Higashi-ku, Osaka, 541

tic moments are determined by using Eq. (1) and are listed in Table I.

Table I. Average magnetic moment of Co and Mn in f.c.c. Co-Mn alloys

at % Mn	T(^{o}K)	μ_{bulk}	$\langle\mu_{Co}\rangle$	$\langle\mu_{Mn}\rangle$
7.6	98	1.45	1.55 ± 0.01	0.27 ± 0.12
7.6	294	1.45	1.58 ± 0.01	-0.16 ± 0.14
15.0	98	1.13	1.29 ± 0.02	0.20 ± 0.11
15.0	294	1.13	1.27 ± 0.01	0.32 ± 0.04
20.0	98	0.91	1.04 ± 0.01	0.41 ± 0.05
20.0	294	0.84	0.96 ± 0.01	0.34 ± 0.05
25.0	125	0.50	0.60 ± 0.03	0.21 ± 0.04
25.0	294	0.37	0.43 ± 0.01	0.20 ± 0.02

Magnetic moments are expressed in unit of Bohr magneton.
Bulk magnetization is cited from J. Crangle; Phil. Mag. 2(1957)659 and J.S. Kouvel: J. Phys. Chem. Solids 16(1960)

It should be emphasized here that $\langle\mu_{Mn}\rangle$ observed in the present investigation is apparently different from that obtained by Cable and Hicks[1] for $Co_{95}Mn_5$, $-(0.97 \pm 0.07)\mu_B$, both in magnitude and orientation. Since their value was obtained for a specimen with different composition and by using unpolarized neutron scattering, it seems to be quite necessary to perform unpolarized neutron experiment for the present specimens.

(ii) Unpolarized neutron experiment

Observed diffuse scattering cross sections are shown in Fig. 1. If we assume that the magnetic moments of $\langle\mu_{Mn}\rangle$ and $\langle\mu_{Co}\rangle$ have the same values as those listed in Table I without any flictuations, the diffuse scattering cross sections can be calculated as shown by dotted curves in the figure. The apparent deviation of these curves from the experimental values implies that there should be moment fluctuations in Mn and/or Co atoms.

(iii) Proposed model

As a magnetic moment of Mn in dilute Co(Mn) alloys, Yasuoka et al [2] have proposed the value of $+3\mu_B$ other than the Cable-Hicks value of $-0.97\mu_B$. Considering these results together with the average value of about $0.2\mu_B$ obtained by the present investigation, we first assume that Mn atoms are in two different states, one of which has the moment of $3\mu_B$ another $-1\mu_B$. Furthermore, we assume that a Mn atom has an antiparallel moment of $-1\mu_B$, if the number of its nearest neighboring Mn atoms with parallel moment is equal to or more than the number of antiparallel Mn atoms. From a condition that the probability of finding the parallel moment at the origin is equal to that at the nearest neighbor site, we can calculate individual magnetic moment of Co and Mn as shown by solid curves in Fig. 2. In this figure experimental values listed in Table 1 are shown by open circles (Mn) and filled ones.

Even though the crude assumptions in the model, the agreement between the both is fairly well, and therefore we can conclude the exsitence of two different moments of Mn in Co-Mn alloys.

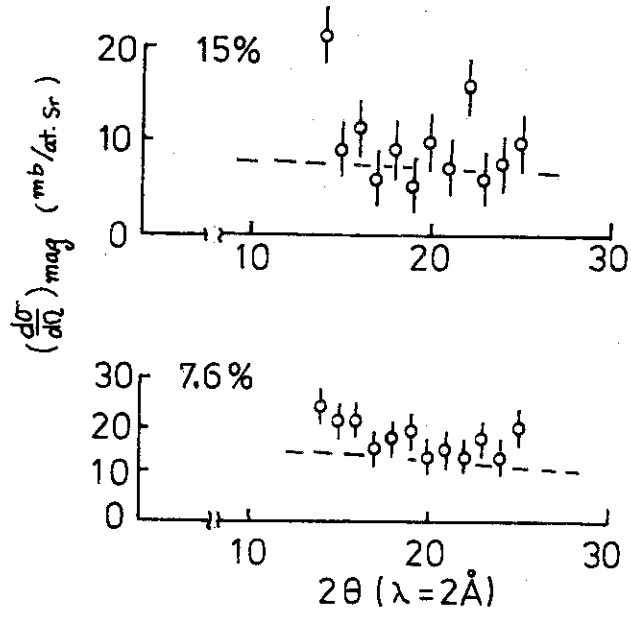

Fig. 1

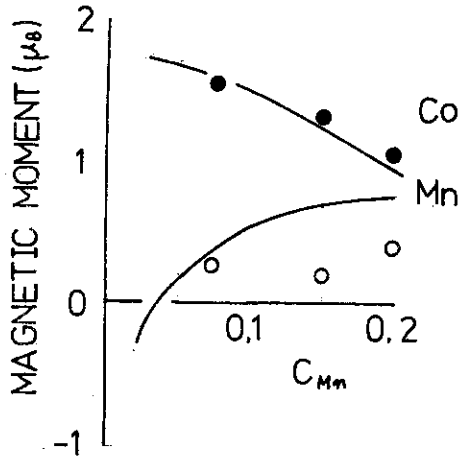

Fig. 2

(1) J.W. Cable, T.J. Hicks Phys. Rev. 2(1970)176

(2) H. Yasuoka, S. Hoshinouchi, Y. Nakamura J. Phys. Soc. Japan 34(1973)1192

Study of Interface Magnetization of Fine Particles Precipitated in Cu

by Masatoshi Sato

(The Institute for Solid State Physics, The University of Tokyo)

Below, the synopsis of the Technical Report of ISSP (Series A, No 823) is cited. For more detailed informations, see the report.

In order to examine the interface effect of Co fine particles precipitated in Cu, experiment of the neutron small angle scattering has been carried out at room temperature. By the analysis of the magnetic scattering intensity normalized by the nucleus one, it can be known that the change of the magnetization of Co atom at the interface is very small, if present. Using the parameters determined by the neutron scattering data the magnetization of Co particles is calculated as a function of magnetic field. Comparing it with the measured data, it is known that even for the very early stage of the precipitation, the particles is consisted of almost pure Co atom.

Neutron Scattering from Paramagnetic MnO

by Hiroshi Betsuyaku (Physics Department)

Manganous oxide (MnO) was the first material that was shown by neutron diffraction methods to be antiferromagnetic at low temperature[1]. It is a typical Heisenberg-type antiferromagnet with the magnetic structure of the second kind of fcc lattice. It exhibits considerable short range ordering of spins well above its Néel temperature of 117K[2]. The inelastic neutron scattering work of Satya Murthy et al.[3] proved the existence of spin-wave-like excitations even in samples at room temperature. The cold neutron scattering study of Kroó and Beta[4] indicated that the spin-wave spectrum above T_N has no abrupt change during the phase transition and evolves continuously into the collective spin excitations in the paramagnetic phase. However both the above-mentioned work used polycrystalline specimens for the time-of-flight neutron scattering measurements and the interpretation of the time-of-flight data is subject to some uncertainties[5].

To get a more direct information of these excitation modes the inelastic scattering from a monocrystalline specimen was measured by using both the time-of-flight and triple-axis methods. The time-of-flight distributions of the scattered neutrons within the (110) plane of reciprocal space of MnO were studied using the pulse-type neutron spectrometer at the JRR-2 reactor at JAERI. The measurements were made in both the paramagnetic and antiferromagnetic regions. At some particular crystal orientations where the scattered wavevectors pass through the (1/2,1/2,1/2) magnetic zone center, discrete peaks due to the spin-wave excitation are found in the time-of-flight spectrum in the antiferromagnetic phase. As the temperature is raised beyond T_N quite well-defined peaks are visible though the intensity of the magnetic Bragg line changes abruptly at T_N. They suffer intensity changes between $1.1T_N$ and $2.0T_N$, but

a trace of excitations still remains above $2.0T_N$. This behavior is shown in Fig. 1. The present time-of-flight data are in qualitative agreements with the result of Kroó and Beta[4].

The behavior of the spin-wave excitations through T_N was measured by using the triple-axis neutron spectrometer at the JRR-2 reactor. Both the constant "Q" and "E" modes of operation were used. It was observed that the spin-wave mode near the magnetic zone center disappears at T_N, but a broad continuous central component appears above T_N which extends over the same energy range as the spin-wave mode exists. This crossover well explains the continuous evolution of the time-of-flight data through T_N. On the other hand, it was observed that the spin-wave mode near the zone boundary suffers a considerable energy decrease with increasing temperature to T_N. It persists well above T_N though it suffers a line broadening. The most striking feature is that this mode persists even at room temperature.

REFERENCES

[1] SHULL,C.G.,SMART,J.S.,Phys.Rev.76(1949)1256.

[2] RENNINGER,A.,MOSS,S.C.,AVERBACH,B.L.,Phys.Rev.147(1966)418.

[3] SATYA MURTHY,N.S.,VENKATARAMAN,G.,USHA DENIZ,K,DASANNACHARYA,B.A., IYENGAR,P.K.,Inelastic Scattering of Neutrons(Proc.Symp.Bombay,1964) 1,IAEA,Vienna(1965)433.

[4] KROÓ,N.,BETA,L.,Inelastic Scattering of Neutrons(Proc.Symp,Copenhagen, 1968)2,IAEA,Vienna(1968)111.

[5] RAO,L.M.,Status solidi(b)50(1971)737.

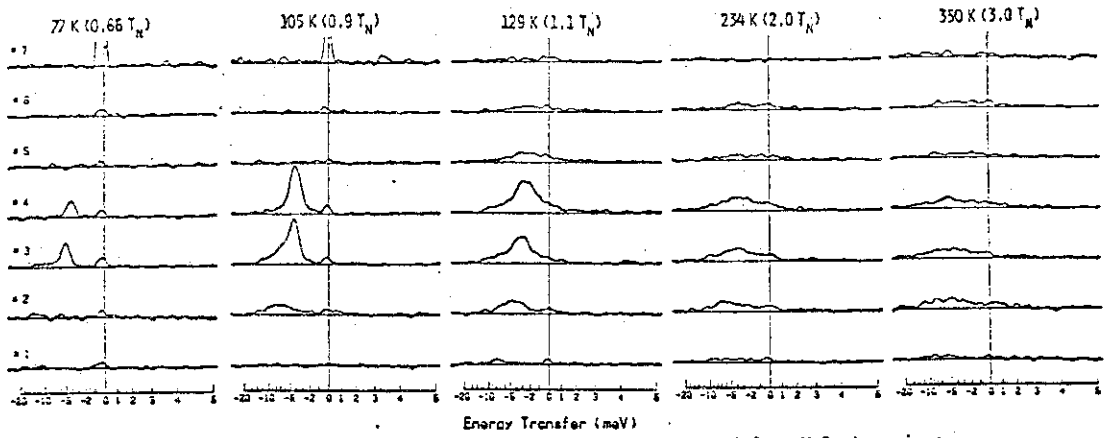

Fig. 1 Time-of-flight spectra of neutrons scattered from MnO at various temperatures using the experimental setting shown in Fig. 2. The numbers from #1 to #7 correspond to the scattering related to the seven different detectors.

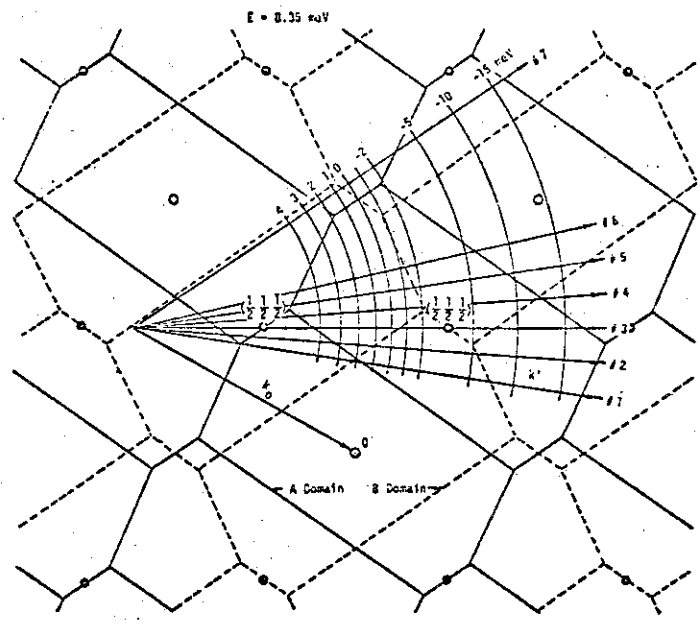

Fig. 2 The reciprocal lattice diagram of MnO in a $(1\bar{1}0)$ plane and a neutron scattering diagram for use in analyzing the time-of-flight spectra of Fig. 1. The incident neutron vector is k_0, and seven lines of scattered vectors k' are shown corresponding to the scattering angles of seven detectors numbered from #1 to #7.

Spin-Wave Dispersion Relations in Mn_2Sb

by Satoru FUNAHASHI (Physics Division, JAERI)

Previously we measured the spin-wave dispersion relations in $Mn_{2-x}Cr_xSb$[1] in which the so called exchange inversion[2] occurs. The remarkable thermal change of the dispersion relation was well interpreted in relation to the thermal expansion of the crystal, by assuming nearly two dimensional magnetic structure.

In pure Mn_2Sb(crystal structure is P4/nmm; T_c=570K), the exchange inversion does not occur. At low temperature, however, it is expected that the interlayer exchange interaction becomes very weak. We measured the spin-wave dispersion relations in this material between 15 and 398K with the spectrometers CTNS and DMNS. The results are shown in Fig.1. The interlayer exchange interactions obtained from the results are corrected for the spin-wave renormalization due to the magnon-magnon interaction and are plotted in Fig.2. It is quite contrary to the expectation described above that the nearest neighbor interlayer interaction increases below 200K. This result cannot be explained in relation to the change of the sign of the anisotropy which occurs at 240K. Another unexpected and strange result is that an intense inelastic neutron scattering appears at q=0 above room temperature as shown in Fig.3. It appears where the magnetic Bragg reflection is present. This excitation seems to be too steep in the q-ω space to be assigned to optical magnons. The excitation energy decreases with increasing temperature. The experiment will be extended to higher temperature shortly.

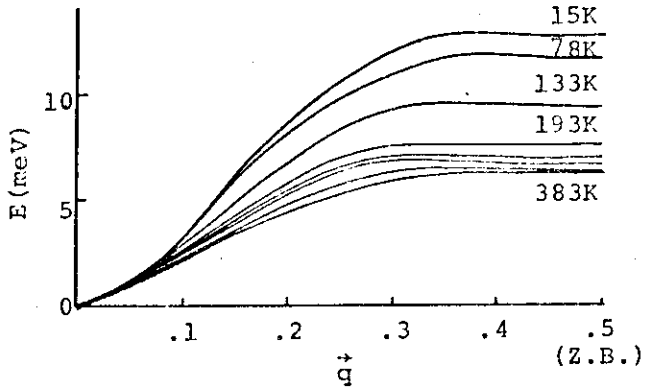

Fig.1 Spin-wave dispersion relations in Mn_2Sb for q// c*.

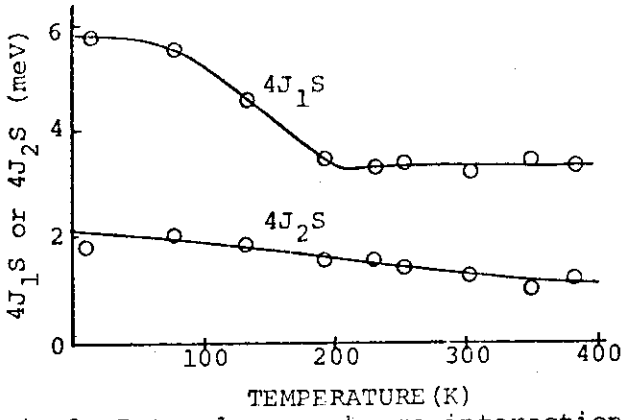

Fig.2 Interplane exchange interactions as functions of temperature. J_1 and J_2 are the exchange integrals between the first and second neighbor planes.

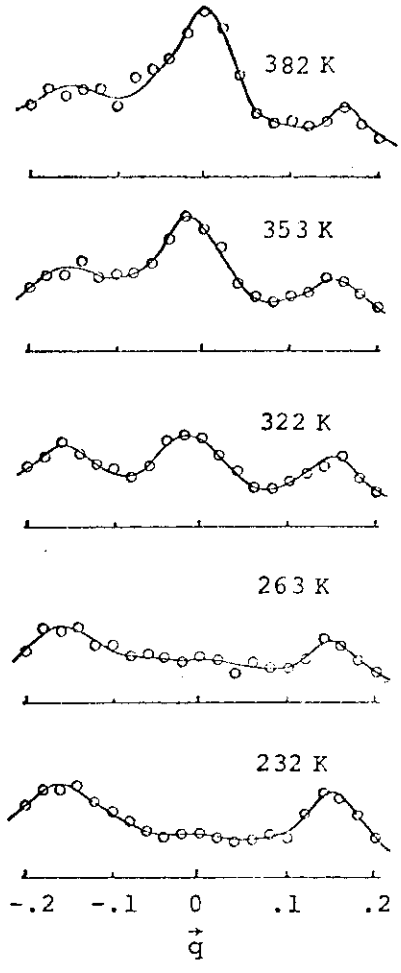

Fig.3 Constant ΔE profile scanned along the [110]-axis with Ei-Ef=25meV. Side peaks correspond to the accoustic magnons.

REFERENCES

1) S.Funahashi and N.Kazama, J.Phys.Soc.Japan 41(1976)811.

2) C.Kittel, Phys.Rev. 120(1960)335.

Spin Waves in TbZn

Yoshikazu Hamaguchi (Phys. Div. JAERI) and
Tsutomu Yashiro (The Institute for Iron,Steel and Other Metals, Tohoku University)

Among the rear earth intermetallic compounds having the CsCl structure, TbCu-TbZn system is well investigated from the point of view of magnetic properties.[1)2)] The appearance of spin-canted structure near middle region has been explained by a mechanism of low concentration electron carrier interaction superimposed on the RKKY interaction. To determine the strength and behaviour of such interactions we need a information of spin wave dispersion relation. First of all spin wave dispersion relations in terminal alloy TbZn have been investigated by using the triple-axis neutron spectrometer. TbZn is ferromagnet which has T_c of 203K and spin direction is <100> above T_f and rotate to <110> below T_f of 65K. It shows strong magnetic anisotropy at low temperature.

Dispersion relations of spin wave have been measured in three principal directions at both 20K and 80K using a single crystal of c.a. 5×5×7 mm. The results are shown in Fig. 1. Anomaly in both <110> and <111> directions suggest the oscillatory behaviour of J(R). Remarkable temperature dipendence of dispersion relation in <100> direction is shown in Fig. 2. Preliminary analysis of those data indicate that the temperature dipendence of spin wave energy can not explain only considering the renormalization of crystalline field anisotropy.

References

1) M. J. Pierre: C.R. Acad. Paris 265 (1967) 1169

2) T. Yashiro Y. Hamaguchi and H. Watanabe: J. Phys. Soc. Japan: 40 (1976) 63

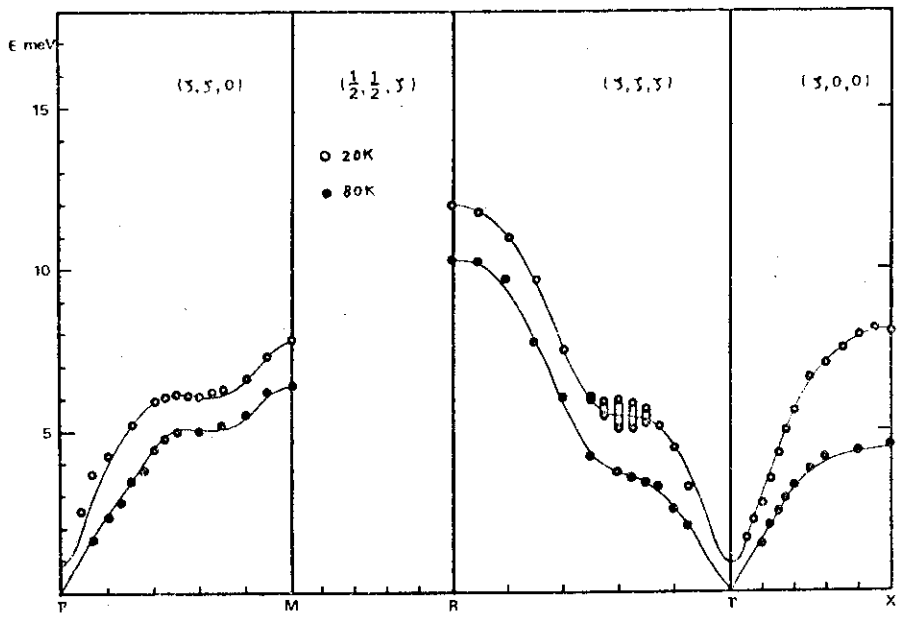

Fig. 1 Dispersion relations of spin wave in TbZn

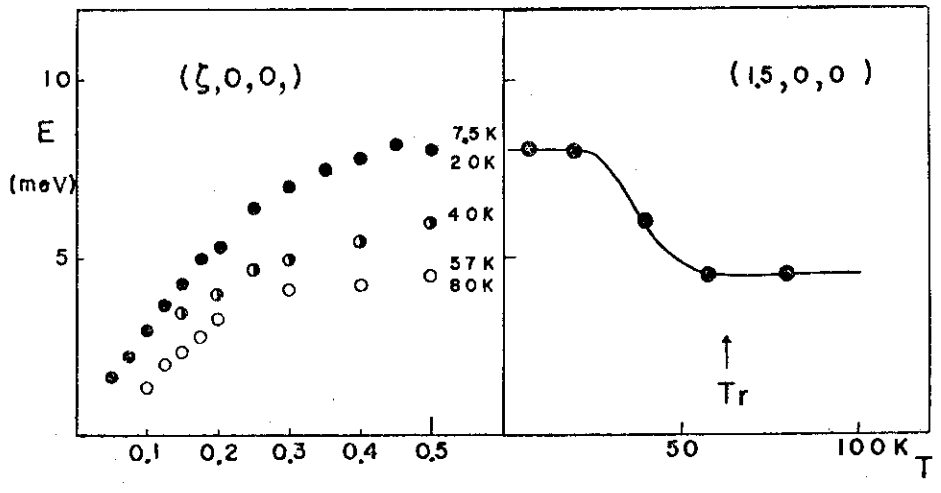

Fig. 2 Temperature dependence of dispersion relation in ⟨ 100 ⟩ direction and zone boundary

Spin Waves in $FePt_3$

by M. Kohgi and Y. Ishikawa
Physics department, Tohoku University, Sendai
and P. Radhakrishna
Institut Laue Langevin, Grenoble

$FePt_3$ is an ordered alloy with the crystal structure of $AuCu_3$ type. Below the temperature of 170 K, it shows an antiferromagnetic ordering which gives $\frac{1}{2}\frac{1}{2}0$ neutron reflections. The magnetic moment of an iron atom is about 3.3 μ_B. Platinum atoms does not have appreciable momenta.[1]

Among many 3d-4d or 3d-5d transition metal alloys which show strong magnetism, $FePt_3$ is a good material to study the strong antiferromagnetism in metal, because it has the simple magnetic structure and the low transition temperature.

We studied the antiferromagnetic spin waves by means of neutron inelastic scattering techniques. The spin wave dispersion below the energy of about 15 meV at 5 K and 77 K were measured on the triple axis spectrometer TUNS at the JRR2 reactor of JAERI. We measured also the high energy part of the dispersion at 5 K on the triple axis spectrometer IN1 at the high flux reactor of ILL.

In fig.1 are shown the results obtained for spin waves propagating along three principal crystal axis. The uncertainties of the peak positions of the spectra are shown by the error bars. The isotropic and linear dispersion realtions hold at small wave vector region, which give the spin wave velocity of about 67 meVÅ and the energy gap of about 2 meV for $q \lesssim 0.16$ Å at 5 K. It is remarkable that the dispersion curves show a distinct decrease of the slope along [110] direction compared to the other directions as the temperature increases from 5 K to 77 K.

We analized the spin wave dispersion curves at 5 K using the Heisenberg type effective spin Hamiltonean, that is $H = \sum_{<ij>} J_{ij}\vec{S}_i\vec{S}_j - \sum_i DS_{iz}^2$, where J_{ij} is the effective exchange interaction between iron atoms and D is the one ion type anisotropy constant. We found that the least square fitting is very poor using less than four

exchange parameteres and not so much improved using more than seven exchange parameters. The obtained best fit values for one anisotropic and six exchange parameteres are:

$D = 0.07$, $J_1 = 2.64$, $J_2 = -1.33$, $J_3 = 1.39$, $J_4 = 0.64$, $J_5 = 0.09$
$J_6 = -0.42$
in the unit of meV.

The calculated dispersion curves using above parameters are shown by the solid and the broken curves in Fig.1. The former correspond to the spin waves in the $[1/2\ 1/2\ 0]$ antiferromagnetic domain to which the wave vector in the figure is refered and the latter correspond to the spin waves in the $[0,1/2,1/2]$ and $[1/2,0,1/2]$ domains which are observed simultaneously. The agreement between the observed and the calculated spin wave spectra is generally good for their peak positions. The widths of the almost all of the spectra, however, are somewhat broader than the calculated. It shows that the life time of the spin wave is finit for wide value of the wave vector even at 5°k.

reference

(1) G. E. Bacon and J. Crangle, Proc. Roy. Soc. A272, 387 (1963)

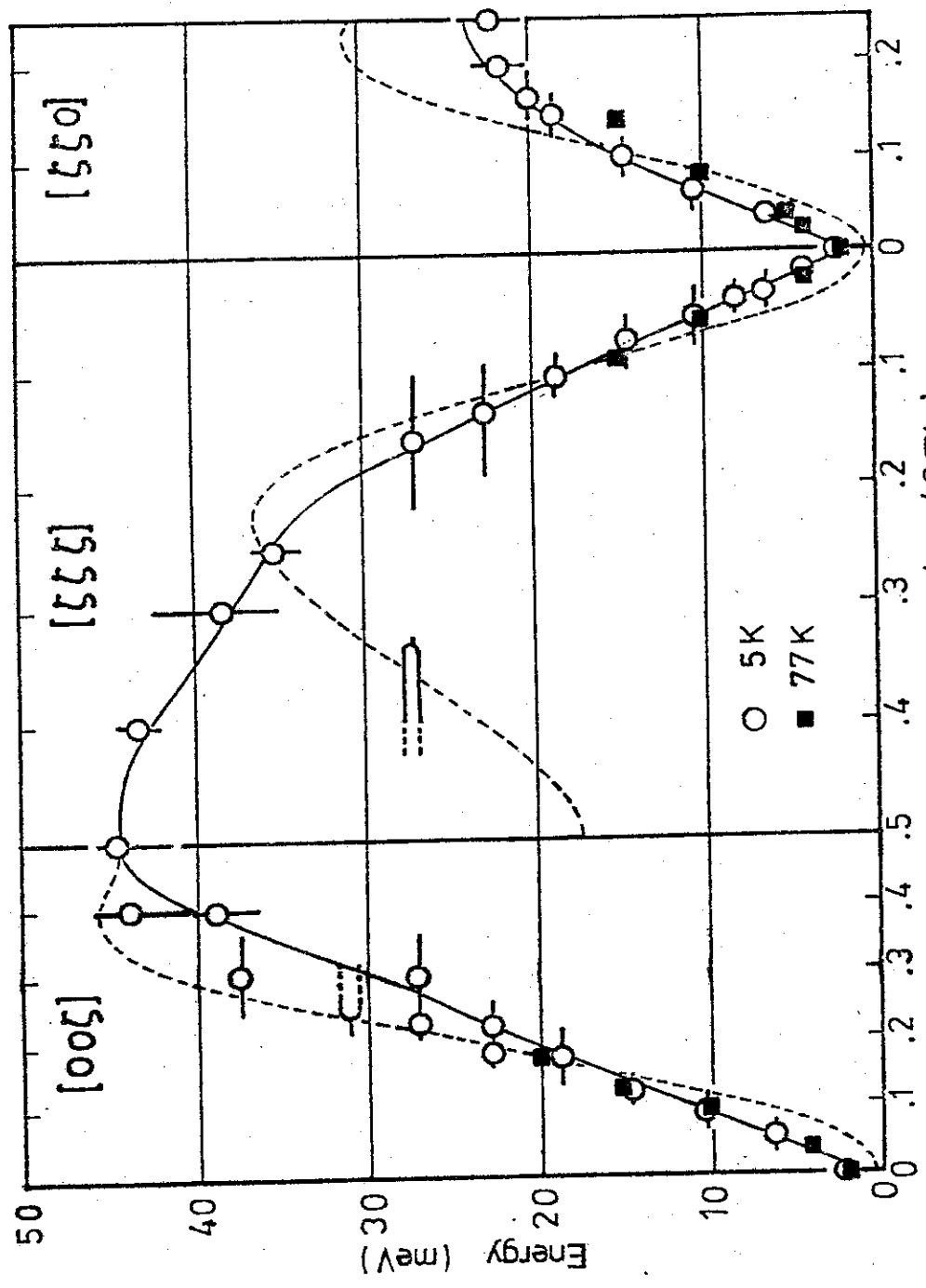

Fig.1 Spin wave dispersion curves of $FePt_3$.

Neutron Spin Wave Scattering Intensities in Fe_3Pt and $Fe_{.65}Ni_{.35}$ Invar Alloys

by Shigefumi Onodera, Keisuke Tajima and Yoshikazu Ishikawa
(Department of Physics, Tohoku University)

Neutron spin wave scattering experiments in Invar alloy give an important information to understand so called "Invar problem". The spin wave excitation is directly connected to the temperature dependence of the spontaneous magnetization which behaves anomalously in an Invar alloy. We measured the temperature dependence of the neutron spin wave scattering intensities of ordered Fe_3Pt and $Fe_{.65}Ni_{.35}$ Invar alloys. Measurements were concentrated to low energy excitation region in which the scattering cross section may be expressed as

$$\frac{d^2\sigma}{d\omega d\Omega} \propto \frac{e^{\hbar\omega\beta}}{e^{\hbar\omega\beta} - 1} \langle Seff \rangle \left[\frac{\Gamma}{\Gamma^2 + (\omega-\omega_{sw})^2} + \frac{\Gamma}{\Gamma^2 + (\omega+\omega_{sw})^2} \right]$$

where Γ is inverse of the spin wave life time and <Seff> is the value corresponding to spontaneous magnetization <Sz>. The experiments were always performed by Constant $\bar{Q}$ mode of operation and the value of Γ and <Seff> were determined by convoluting the cross section formula with resolution function. In Figs.1 and 2, we show the temperature dependence of <Seff> and Γ for Fe_3Pt and FeNi. <Seff> is normalized to the value of the lowest temperature. Dotted lines in Fig.1 represent <Sz> obtained from magnetization measurements. The temperature dependence of <Seff> and <Sz> does not coincide with each other in both samples. These results are contrast with the Heisenberg ferromagnetic metal Pd_2MnSn in which the temperature dependence of <Seff> and <Sz> coincides with each other. The value of Γ in Fe_3Pt and FeNi increases linearly with increasing temperature and gives $\sim$1 meV near T_C, which is twise as large as that of Pd_2MnSn. Above T_C, we observed a spin wave like excitation at small momentum transfer region. These anomalous behavior of spin wave excitation might be interpreted in terms of the inhomogenuity in Invar alloys.

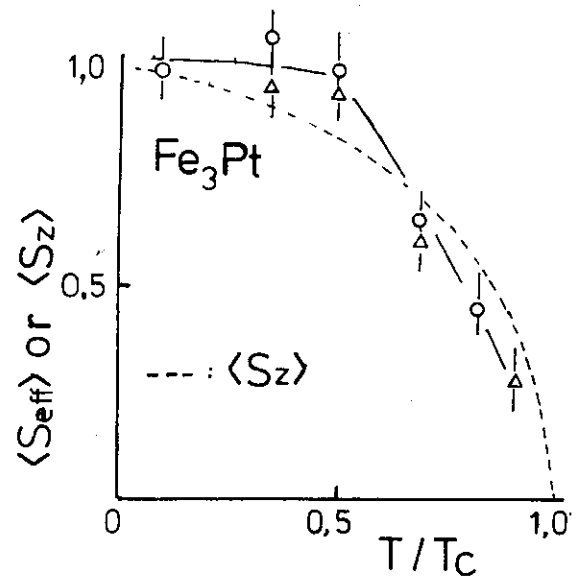

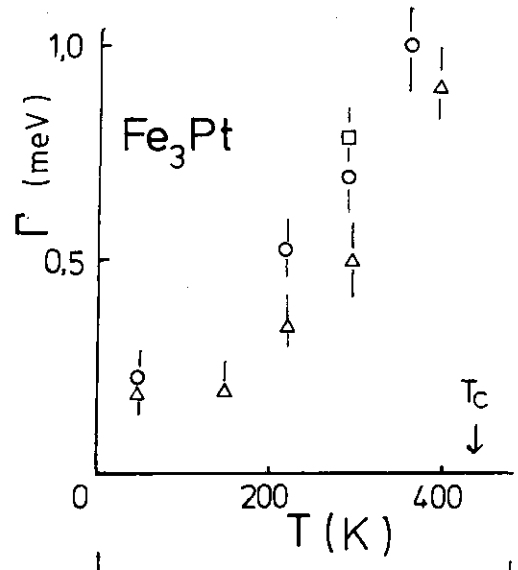

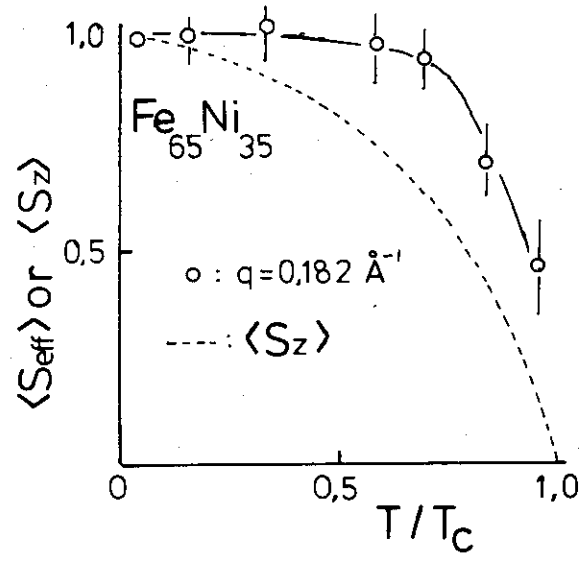

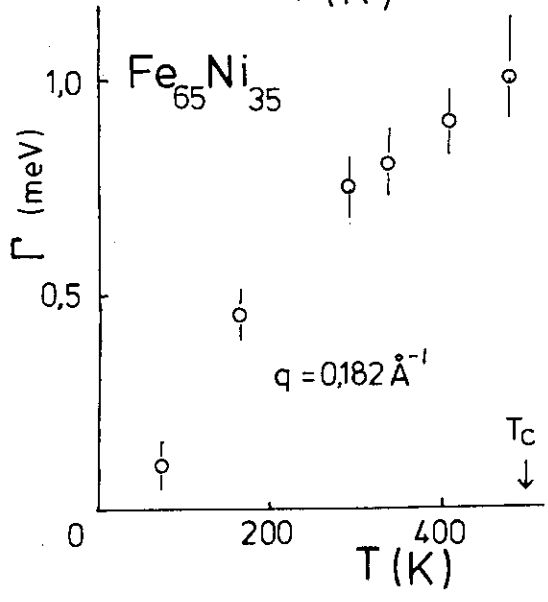

Fig. 1
The temperature dependence of <Seff> and <Sz> in Fe_3Pt and $Fe_{.65}Ni_{.35}$.

Fig. 2
The temperature dependence of Γ in Fe_3Pt and $Fe_{.65}Ni_{.35}$

Magnetic Excitation of Fe-V Alloy

Noboru SCHIBUYA, Yutaka NAKAI and Nobuhiko KUNITOMI
Faculty of Science, Osaka University, Toyonaka
Osaka, 560

In view of recent advances in the experiment and the theory of the spin dynamics in disordered alloy systems very few works have been done except on Fe-Ni alloy system. Thus the need for extensive experimental data is obvious.

In dilute alloy weakly bound magnetic impurity atom might cause the effect on the spin wave spectrum of the host atom to yield the resonance spin wave mode.[1] In concentrated alloy such a resonance mode, i.e. the gap of the spin wave density of state, also can be expected as already observed in phonon spectrum in Pt-Ni alloy system.[2]

In the present work magnetic excitation spectrum of Fe-V 13.5at% alloy has been studied by coherent inelastic neutron scattering. The Curie temperature of the ferromagnetic Fe-V alloy is about 990k. The atomic magnetic moments of its constituent atoms are reported as μ_{Fe}= 2.0 μ_B and μ_V=0.8 μ_B by Yamashita et al.[3], the directions of which are antiparallel with each other.

(i) Sample preparation

Sample was prepared from raw materials of 99.95% Fe and 99.95% V. An ingot melted in an induction furnace was remelted and grown to a single crystal by the Bridgeman method. The size of the sample is 10mmϕx 25mm .

(ii) Experiment and Result

The measurements were performed with the TUNS-triple axis spectrometer at JRR-2. Single crystal was mounted with the [1$\bar{1}$0] crystallographic axis vertical at R.T. and all measurements were made on spin waves propagating in the [00ζ] direction around (110) Bragg reflection. A neutron beam of fixed energy E_o=33.6 meV was incident on the sample and the distribution of scattered neutrons was measured with the constant energy transfer modes of operation.

Observed spectra of Fe-V 13.5% for the energy transfers at 8, 9, 10, 12, 16 and 20 meV are shown in figure 1. The width of each spectrum roughly agrees with that of the resolution function, except that the width of the spectra of the spin wave transfers of 9 and 10 meV was slightly wider than the others. The intensity distribution map of scattered neutron groups was drawn on the ω-K plane as shown in figure 2.

Assuming the dispersion relation as $h\omega=DK^2$ the stiffness constant was obtained as $D=370\pm40$ meV A^2 which is large compared with that of Fe, the value of which agrees with that, $D=400$ meV A^2, obtained with Diffraction method by Lowde et al.[4]

The dispersion curve shows a striking anomaly near the spin wave energy of 10 meV, the reason of which has been not yet understood, however, it seems to be the effect of the weakly bound atom to the spin wave spectrum. Theoretical investigation based on both the Heisenberg model and the band model is now developed.

Farther experiment with other samples of the different Vanadium concentration 7.6 at% V and 19.0 at% V is in progress.

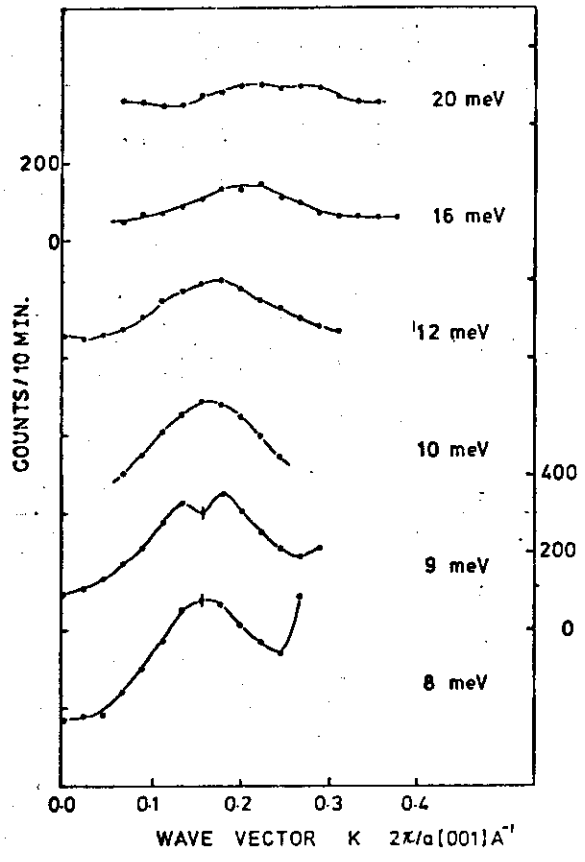

Fig. 1
The distribution in wave vector transfer scattered neutrons from FeV 13.5 % at 293 K observed in constant energy scans at 8, 9,10,12,16 and 20 meV

(1) N.Kroó and L.Pal JAP 39 453 (1968)
T.Wolfram and J.Callaway Phys.Rev. 130 2207 (1963)
(2) Y.Tsunoda, N.Kunitomi, N.Wakabayashi, R.M.Nicklow and H.G.Smith
private communication
(3) O.Yamashita, Y.Yamaguchi and H.Watanabe to be published in JPSJ
(4) R.D.Lowde, M.Shimizu, M.W.Stringfellow and B.H.Torrie
Phys.Rev.Lett. 17 698 (1965)

FIG. 2

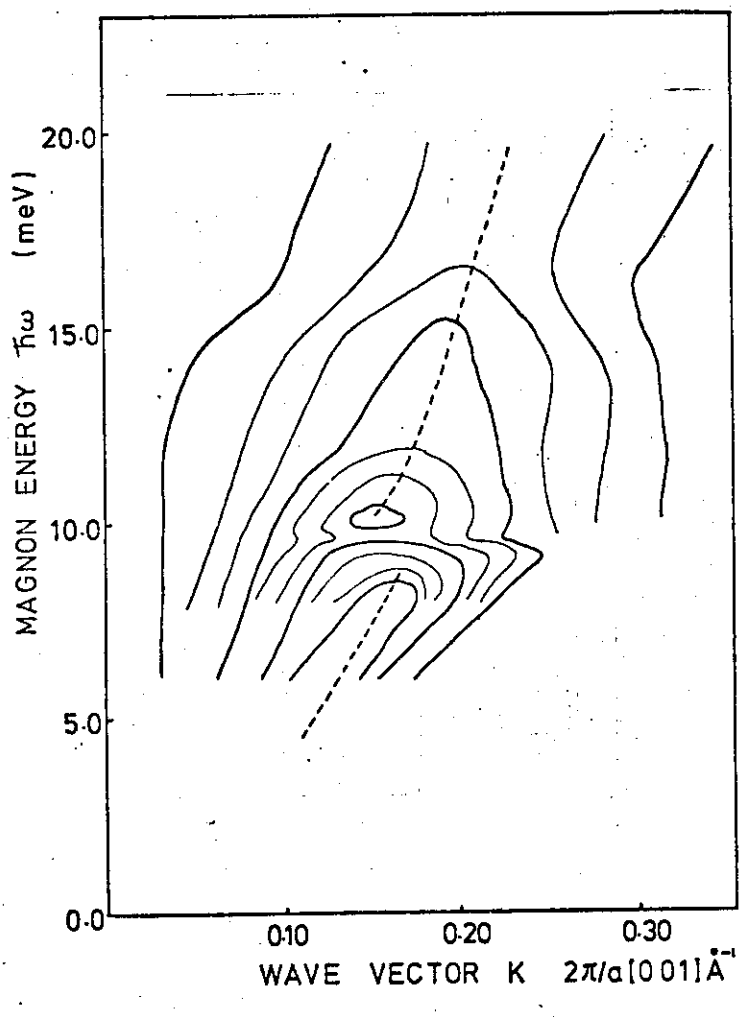

Fig.2
Contour diagrum of the intensity in the ω-K plane. The contours were drawn by eye through all the experimental points.

ADDENDA - The experiment was reexamined by using the TAS at HFIR in Oak Ridge National Laboratory but the resonance mode as observed here was not confirmed althogh the observed values are consistent with the present ones within the statistical error. We have to conclude that the anomaly observed here is due to the lack of the statistical accuracy in the present experiment.

QUASI-ELASTIC NEUTRON SCATTERING OF IONIC SOLUTIONS

T. Sakuma, S. Hoshino and Y. Fujii
Institute for Solid State Physics, The University of Tokyo
Roppongi, Minato-ku, Tokyo 106

When a salt is dissolved in water, there are at least three types of protons experiencing different interactions. These would be protons in the neighbourhood of positive ions, those near negative ions and those relatively far away from any solute ions. In this case, it is important to analyze not only a FWHM of energy spectrum of scattered neutrons, but also a whole shape of the spectrum.

Quasi-elastic neutron scattering of ionic solutions ($AlCl_3$, $NiCl_2$, NaCl, KI etc.) was measured using the ISSP ND-1 triple-axis spectrometer with the wavelength of 2.44 Å from PG(002) double-monochromator system. The observed energy spectrum of $AlCl_3$ solutions at $Q^2 = 5$ ($Å^{-2}$) is shown by open circles in Fig.1. This spectrum consists of two components. One of them is of Gaussian-like (dotted curve in Fig.1) and the intensity increases with increasing concentration of $AlCl_3$. The other contribution is almost the same as that of pure water (shadowed part in Fig.1). It is found that the dynamical properties of a certain part of water molecules bound to Al ions is different from the remaining. Other solutions have also been studied by the same method of the analysis.

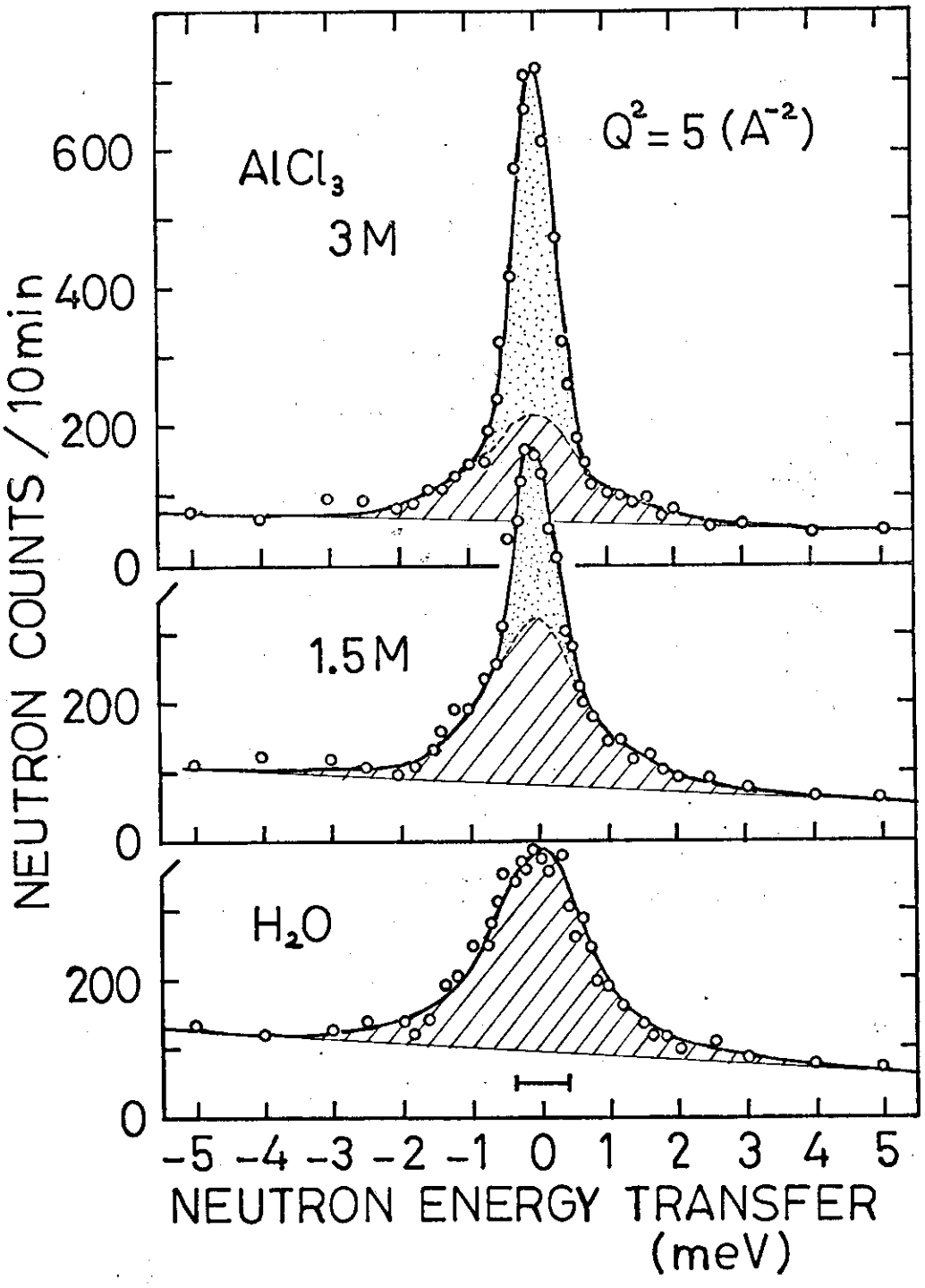
$Q^2 = 5\ (A^{-2})$
$AlCl_3$
3M
1.5M
H_2O
600
400
200
0
200
0
200
0
NEUTRON COUNTS / 10min
-5 -4 -3 -2 -1 0 1 2 3 4 5
NEUTRON ENERGY TRANSFER
(meV)

Fig. 1

Slow Neutron Polarization by Polarized Proton Filter Using Ethylene Glycol

S.Hiramatsu, S.Isagawa, S.Ishimoto, A.Masaike, K.Morimoto (National Laboratory for High Energy Physics),
S.Funahashi, Y.Hamaguchi, N.Minakawa (JAERI),
Y.Yamaguchi (The Research Institute for Iron, Steel and Other Metals, Tohoku University)

Polarized proton system has been expected to be good polarrizing neutron filter for wide spectrum neutron beam. Not only high polarization of the neutron but also high transmission of the beam is desired of an efficient filter.

We tested ethylene glycol filter doped with $K_2Cr_2O_7$, with the polarized neutron diffractometer POLTO. The merits of ethylene glycol are high proton density and easiness of the sample preparation. Protons in the ethylene glycol were dynamically polarized in the magnetic field of 25kOe with the microwave of 70GHz. The thickness of the filter was 9.6mm. The temperature of the filter was 0.3K in the absence of microwave, and was 0.45K with microwave pumping. The maximum proton polarization was 72%. The polarized neutron beam(λ=1Å) from POLTO was guided to the filter and the transmitted beam intensity was measured without polarization analysis. The polarization of the incident beam was inverted periodically. Fig.1 shows the corresponding periodic change of the transmitted neutron beam intensity. Fig.2 shows the neutron polarization efficiency of the 9.6mm thick ethylene glycol calculated from the present results. The maximum polarization efficiency was 84%.

It is concluded from the present experiment that ethylene glycol is promising for practical use as the efficient polarizing neutron filter. The experimental details and the analyses including the estimation of the transmission efficiency will be published soon.

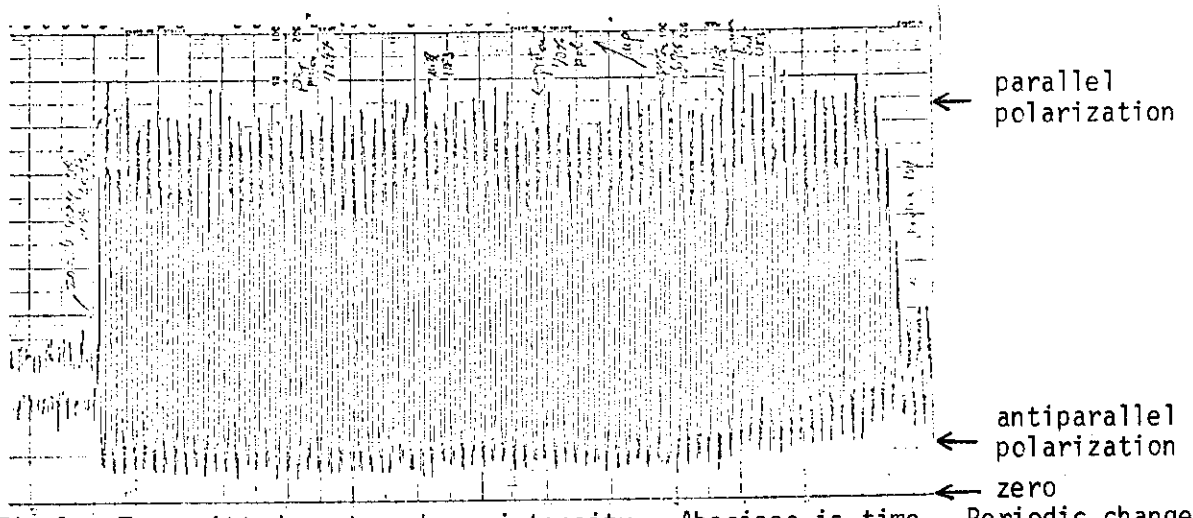

Fig.1. Transmitted neutron beam intensity. Abscissa is time. Periodic change of intensity corresponds to the incident neutron polarization inversion.

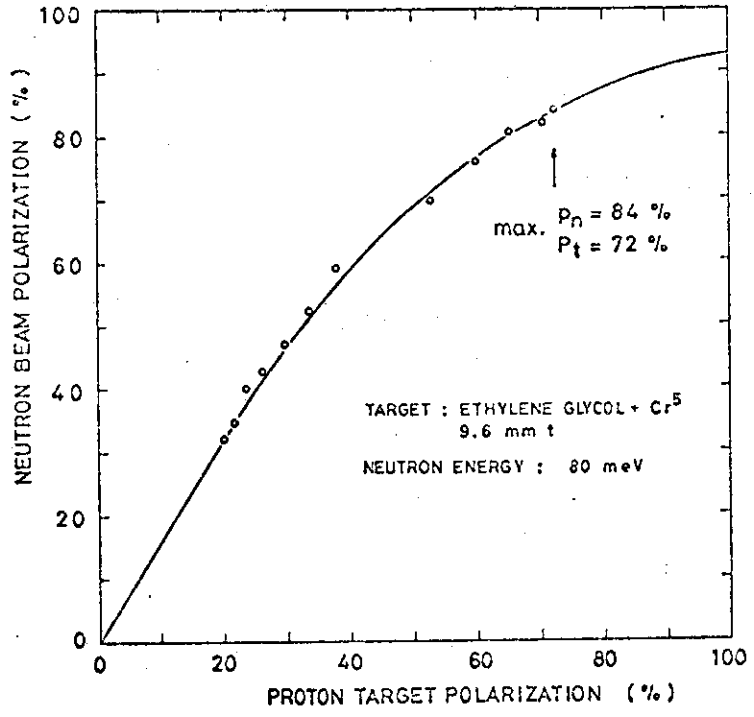

Fig.2. Neutron polarization efficiency of 9.6mm thick ethylene glycol filter as a function of proton polarization.

Bragg Reflection from the Multilayer of Fe-SiO Films

by Masatoshi Sato

(The Institute for Solid State Physics, The University of Tokyo)

and

Keizō Murata* and Kazushige Nomura

(Department of Physics, The University of Tokyo)

For the scattering studies using the spin polarized neutron beam, it is desired to produce the polarizer or analyzer with a better efficiency than those which exist now. The reflection from the multilayer (ML) of the ferromagnetic material and other one has been studied in such a purpose[1]. Since the width W of the reflected beam from ML is $\sim L\theta$, to obtain the enough value of W for the practical value of L, the length of ML, we have to make the scattering angle 2θ as large as possible. For the Bragg reflection, θ is inversely proportional to the superlattice spacing D of the ML and therefore it is required to make the films as thin as possible. Taking into account these facts, we have made a Fe-SiO ML by a vacuum evaporation technique on the mylar substrates attached to Cu plate which is held at 77°K and observed the Bragg reflection from it.

It is emperically known that by using the evaporation on the substrate at room temperature, we cannot obtain homogeneous thin films but the agglomerated particles and that therefore for the specimen thinner than the critical thickness d_c (> 50 Å

*present address, Electrotechnical Labolatory

for Fe), the appreciable conductivity of the electron does not exist. On the other hand, the films made by the evaporation on the cooled substrate in which case atomic diffusion does not take place during the evaporation, can be considered to be homogeneous within the statistical error of the piled atom number. We can expect that the specimen made by the successive evaporation on the cooled substrate forms the superlattice structure.

The 40 pairs of Fe-SiO were evaporated in the vacuum of 1×10^{-6} torr. The thicness of Fe is about 30 Å and that of SiO is about 60 Å. By the simple calculation the following relation can be obtained.

$$g_{Fe,n} - g_{SiO} = g_{Fe,m}$$
$$\left|(g_{Fe,-} - g_{SiO})/(g_{Fe,+} - g_{SiO})\right|^2 = 0(10^{-4})$$
$$g_{Fe\pm} = g_{Fe,n} \pm g_{Fe,m}$$

where $g_{Fe,n}$, $g_{Fe,m}$ and g_{SiO} are the scattering anplitude density for the nucleus and magnetic contributions of Fe, and SiO, respectively. From these relations, it can be expected that the reflected beam from this ML is highly polarized. The observed Bragg peak of the first order is at the scattering angle of 1.5° for λ=2.44 A.

The figure shows the observed peak intensity as a function of the applied magnetic field H which is perpendicular to the film. It is normalized by the sum of the nuclear and magnetic scattering contributions. For $H\to\infty$, it tends to about 0.5.* This fact indicates that the polarization of the reflected beam is nearly perfect.

Since the mylar film was attached to the Al plate during the experiment, the mosaicness was rather large due to the undulation

*The demagnetization field of this specimen seems to be smaller than that of the ideal Fe film by a factor of 2/3. It may be due to the inhomogeneity of the Fe films.

of the mylar. The full width of half maximum is about 0.6°. The peak reflectivity of the beam narrower than this mosaicness is about 1.5 % for the unpolarized beam and 3.0 % for the polarized beam.

For the present sample, the required length to obtain the W value of 1 cm is about 35 cm for λ = 5.0 Å. This length is not so unpractical. Let us note that in contrast to the present case the most intense reflection can be obtained with the condition of $d = \frac{D}{2}$ for a given D. We believe that this condition is favourable to make more homogeneous Fe films and that the improvement of the reflectivity can be done because in the present case the degree of the homogeneity of Fe film must detremine the reflectivity. Many trials on this problem will be continued by us in the future.

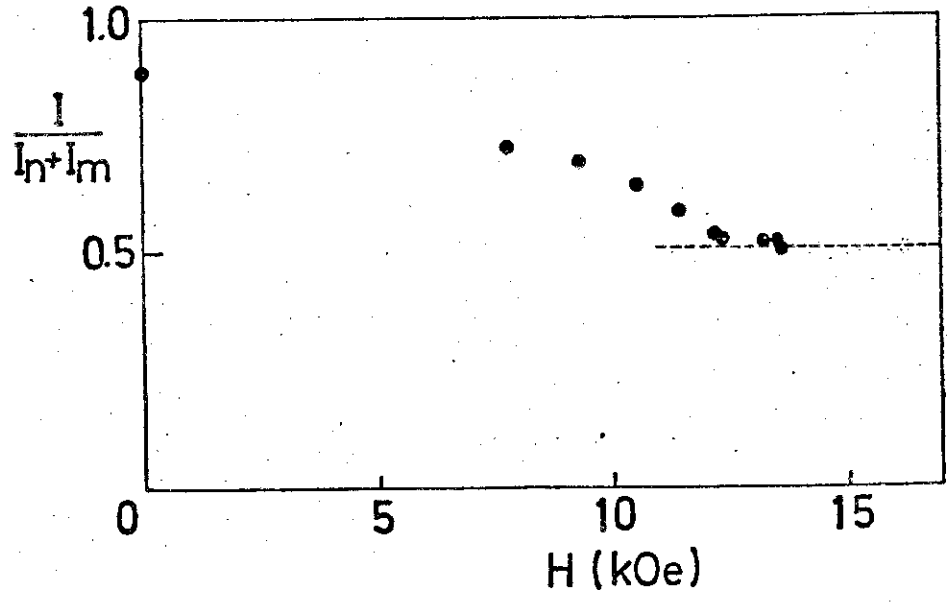

1) B. P. Schoenborn, D. L. D. Caspar and O. F. Kammerer: J. appl. Cryst. 7 (1974) 508 ; J. W. Lynn, J. K. Kjems, L. Passell, A. M. Saxena and B. P. Schoenborn: J. appl. Cryst. 9 (1976) 454.

NEUTRON DIFFRACTION TOPOGRAPHIC OBSERVATION OF A SINGLE CRYSTAL OF Cu-5%Ge SOLID SOLUTION#)

by

Hiroshi TOMIMITSU, Kohji KAMADA and Kenji DOI (JAERI)

(Abstract)

Specimen crystal is a solid solution of Cu-5%Ge alloy with cylindrical shape of 30 mm in diameter and 95 mm in length, which is prepared by the Bridgman method with growth axis nearly parallel to [110] direction. On the specimen surface, there are visible three kinds of successive striations, which are proved, by X-ray Laue photography, to correspond the traces of the three kinds of {100} planes on the specimen surface. Internal textures of the specimen crystal are observed by neutron diffraction topography[1,2] and the existence of {100}-irregularity throughout the Cu-5%Ge single crystal is disclosed. This irregularity may be caused by the periodic segregation of Ge atoms in the alloy. Detailed studies are now in progress.

(References)

#) This investigation is orally represented at the annual meeting of the Crystallographic Society of Japan (1977, Tokyo).

1) K.Doi, et al: J. Appl. Cryst. 4, 528 (1971).

2) H.Tomimitsu and K.Doi: J. Appl. Cryst. 7, 59 (1974).

Neutron Diffraction by JAERI Linear Accelarator

Masanobu Sakamoto and Haruhiko Motohashi

(Physics Division, Japan Atomic Energy Research Institute)

A neutron time-of-flight diffractometer has been set up at the JAERI-Linac pulsed neutron source. Fast neutrons are produced through the (γ,n) reactions with the emission γ-ray by 100Mev electrons in the target, which consists of tantalum and lead plates separated by gaps for cooling water. In usual operations, 150 pulses per second are incident on the target, about 5kw of beam power are absorbed and $\sim 10^{13}$ fast neutrons per second are generated.

The fast neutrons are moderated by slabs of polyethlene (16×16 ×3 cm^3) placed adjacent to the targets, and nearly normal to the flight tube for neutrons. The moderators consist of 10 mm polyethylene slabs separated by a 0.5 mm cadmium sheet from 20 mm polyethylene slabs of the target side. The composition and dimensions have been optimised for the study of powder samples. By using the heterogeniously poisoned moderators with cadmium sheet, a resolution figure $\Delta d/d \gtrsim 0.01$ can be achieved over a rang of d-spacing 0.5 A to 2 A.

The incident neutrons pass through a tapered collimator in the shielding wall, and strike the sample situated at a center of sample table with diameter 50 cm, which can rotate continuously. The maxmum beam size at the sample is reduced to 25×40 mm^2 by means of a collimator. The scattered neutrons from the sample impinge on the counters situated on the circular table of diameter 120 cm with inner diameter 50 cm which can rotate independently of the sample table. The counter block consists of two 25 mm diameter × 250 mm

long He^3 counters and covered a solid angle~0.02 steradians. In the diffractometer, the initial and final flight paths are L_1=5.58 m and L_2=0.75 m.

Figure shows a diffraction pattern from ~70 gms of nickel. Closely spaced (531) ($S=h^2+k^2+l^2=35$, d=0.596 A) and (600), (442) (S=44, d=0.587 A) are resolved. The wavelength distribution of the incident neutrons has been measured from the scattering data on a vanadium sample. Profile fitting of the pattern over a range of d-spacing from 0.5 to 2 A is going on.